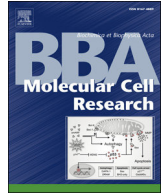




Contents lists available at ScienceDirect

Biochimica et Biophysica Acta

journal homepage: www.elsevier.com/locate/bbamcr

Q2 Dual-laser homo-FRET on the cell surface

Q3 László Bene^{a,*}, Tamás Ungvári^b, Roland Fedor^a, István Nagy^c, László Damjanovich^a3 ^a Department of Surgery, Medical and Health Science Center, University of Debrecen, Debrecen, Hungary4 ^b Department of Biophysics and Cell Biology, University of Debrecen, Medical and Health Science Centre, Faculty of Medicine, Hungary5 ^c Division of Electronics, Research Center for Nuclear Physics of the Hungarian Academy of Sciences, Debrecen, Hungary

6 ARTICLE INFO

7 Article history:
8 Received 24 July 2014
9 Received in revised form 19 January 2015
10 Accepted 2 February 2015
11 Available online xxx

Q4 Keywords:

13 Inhomogeneous broadening
14 Solvent relaxation
15 Red-edge effect
16 Blue-edge effect
17 Directed energy migration FRET
18 Fluorescence anisotropy
19 Fluorescence polarization
20 Rotational mobility
21 Proximity
22 Receptor association
23 Receptor cluster
24 Flow cytometry
25 Fluorescence anisotropy lifetime imaging
26 microscopy (rFLIM)

ABSTRACT

Inhomogeneous broadening and red-edge effects have been detected on a highly mobile system of fluorescently 27 conjugated mAbs targeted to cell surface receptors. By exploiting site-selective spectroscopy and the character- 28 istic loss of homo-FRET on increasing excitation and decreasing emission wavelengths, contributions of physical 29 rotation and homo-FRET to the depolarization of fluorescence anisotropy have been separated. Absolute homo- 30 FRET efficiency has been determined by ratioing two anisotropies: a homo-FRET-sensitive one, which is excited 31 at the absorption main band and detected at the long wavelength region of emission, and a homo-FRET- 32 insensitive one, which is excited at the long wavelength region of absorption and detected at the short wave- 33 length region of emission. Because the anisotropies are simultaneously detected in a unified detection scheme 34 of a dual T-format arrangement, the method is applicable for the real-time tracking of dynamical changes of 35 physical rotations and proximities. The utility of the method is demonstrated in the context of the MHCII mole- 36 cule and the heavy and light chains of the MHC I molecule, a system of three receptors with well-characterized 37 close mutual proximities. Although the method is presented for a flow cytometer, it can also be realized in a fluo- 38 rescence microscope capable for dual-laser excitation and dual-anisotropy detection. 39

© 2015 Published by Elsevier B.V.

42

43

44

1. Introduction

46 Homo-energy transfer (homo-FRET) is an important phenomenon 47 for detecting and quantifying receptor clusters in the 1–10 nm inter- 48 receptor separation range by using a single type of fluorophore [1–9]. 49 Generally it is measured through its depolarizing effect exerted on the 50 fluorescence anisotropy. Because possible rotational Brownian-motion 51 of the fluorophores could also contribute to depolarization of anisotropy, 52 homo-FRET can most readily be detected for systems possessing 53 highly restricted rotational mobility on the nsec time-scale, e.g., differ- 54 ent kinds of visible fluorescent proteins (VFPs) [1,10,11]. In the more 55 general case of fluorophores having substantial rotational mobility, a 56 common way of separating the effects of homo-FRET and rotational 57 motion is changing the concentration of fluorophores by either applying 58 different amounts of dyes for labeling or by photobleaching [12,13]. The

limitations of these approaches are that they require multiple samples 59 and/or they are not reversible precluding real time monitoring of 60 dynamic processes when both proximity and mobility can change 61 simultaneously. Additionally photobleaching may be applied mainly in 62 microscopy rather than flow cytometry due to the required high light 63 doses. A reversible way of depressing homo-FRET may be absorption 64 saturation, but this may require high illumination intensities which 65 may interfere with life processes [14]. 66

Aiming at the generalization of the approach set out by A. Squire 67 et al. [10] – who measured homo-FRET between practically immobile 68 VFP chromophores – for systems having larger degree of rotational 69 mobility than VFP, we propose an alternative method for the isolation 70 and the optimization of the detection of homo-FRET. It is accomplished 71 by exploiting the characteristic wavelength dependencies of homo- 72 FRET, i.e., the absorption red-edge and emission blue-edge effects [11, 73 15–20], shown in the presence of inhomogeneous broadening. 74

Inhomogeneous broadening is the phenomenon when the molec- 75 ular energy levels become distributed due to different interaction 76 strengths with the local environment, such as solvent shells, protein 77 and lipid milieus. Because the energy levels of different molecules are 78 affected differently, this broadening is called inhomogeneous, in con- 79 trast to the homogeneous broadening when the energy levels of all 80

Abbreviations: FRET, fluorescence resonance energy transfer; MHC I/MHCII, Class I/Class II Major Histocompatibility Complex protein; β_2m , beta-2 microglobulin, the light chain (Lc.) component of MHC I; mAb, monoclonal antibody

* Corresponding author at: Department of Biophysics and Cell Biology, University of Debrecen, H-4012 Debrecen P.O. Box 39, Hungary. Tel./fax: +36 52 412 623.

E-mail address: bene@med.unideb.hu (L. Bene).

<http://dx.doi.org/10.1016/j.bbamcr.2015.02.001>

0167-4889/© 2015 Published by Elsevier B.V.

molecules are affected the same fashion (e.g., vibrational- or thermal-broadening, velocity- or Doppler-broadening, natural-broadening of spectra). While the deeply lying energy levels are occupied by the most strongly interacting particles, the upper lying levels are occupied by the weakly interacting ones. In the method called site photoselection, it is possible to monitor only a specified subpopulation of the total one at custom according to the strength of interaction with the environment. This is achieved with narrow-band light sources tuned in wavelength to the energy of the subpopulation in interest. Specific, environment sensitive “2-state” dyes working on these principles have developed recently for monitoring fluidity gradients in membranes, membrane surface potential, dipole potential, and lipid phase transitions (“potential and fluidity probes”, “polarity dyes”) [17–19]. Because FRET is governed by the spectral overlap between absorption and emission spectra, molecular rendering according to energy levels introduces directionality in FRET, implying energy migration in the direction of decreasing energy (Fig. 1, Panel A) [20]. The absorption red-edge effect – discovered by G. Weber in 1960 [16] – and the emission blue-edge effect are consequences of this general principle, and they refer to failure of FRET due to the depletion of energy acceptors and donors for FRET, respectively (Fig. 1, Panel B).

Concerning first the absorption red-edge effect, elimination of the effect of rotational depolarization may be attempted by ratioing two anisotropy values simultaneously measured at the maximum and at the long wavelength edge of the absorption spectrum (red-edge), the latter anisotropy being dependent only on rotation, while the former being dependent on both homo-FRET and rotation. The emission counterpart of this phenomenon, called the blue-edge effect, also exists: While the anisotropy detected at the maximum of the emission spectrum is affected by both rotation and homo-FRET, the one detected at the short wavelength emission edge (blue-edge) is affected by only rotation, thereby offering another possibility for the elimination of the effect of rotation by ratioing two appropriate anisotropies. By combining these two effects for increasing efficiency, we aimed to separate rotation and homo-FRET by sequentially photoselecting a subpopulation sensitive mainly to rotation, accomplished with red-edge excitation, blue-edge emission, and another one equally sensitive for both rotation and homo-FRET, accomplished with main-band excitation, red-edge emission, in a flow cytometer. Besides the spectral heterogeneity, and directionality in FRET however, heterogeneities in other spectral characteristics such as fluorescence lifetime and rotational correlation time, may also arise, which can be taken into account in a calibration procedure.

We first demonstrate the existence of the red-edge effects for the surface-tethered dyes. Then we show the feasibility of a hybrid approach which takes into account both the aforementioned red-edge and blue-edge effects for an efficient separation of the depolarizing effects of homo-FRET and rotation in flow cytometric dual-laser dual-anisotropy homo-FRET determinations in clusters of the MHC I and MHC II molecules. These are two important cell surface immune receptors vital in the initiation of T-cell mediated immune responses [4,21]. The receptors were labeled with fluorescently stained mAbs. Practical questions such as sensitivity of the method to the strength of homo-FRET, the dye's tethering motion, and segmental flexibility of the dye-docking protein moieties have been addressed by applying different types of fluorophores such as Alexa Fluor-488 (A488) and the highly mobile xFITC, a dye with a 7-atom spacer, for staining the Fab portions as well as the whole versions of mAbs at different dye/protein labeling ratios. The significance of the approach is that it enables the separation the depolarizing effects of homo-FRET and rotational motion, i.e., it enables the simultaneous estimation of proximity and rotational mobility of receptors by using only a single cell sample in steady state conditions. The fact that the extent of rotational motion can be estimated besides FRET may gain special importance, because it may offer the feasibility for the estimation of orientation factor (κ^2) and consequently the distance from the measured homo-FRET efficiencies [22–24].

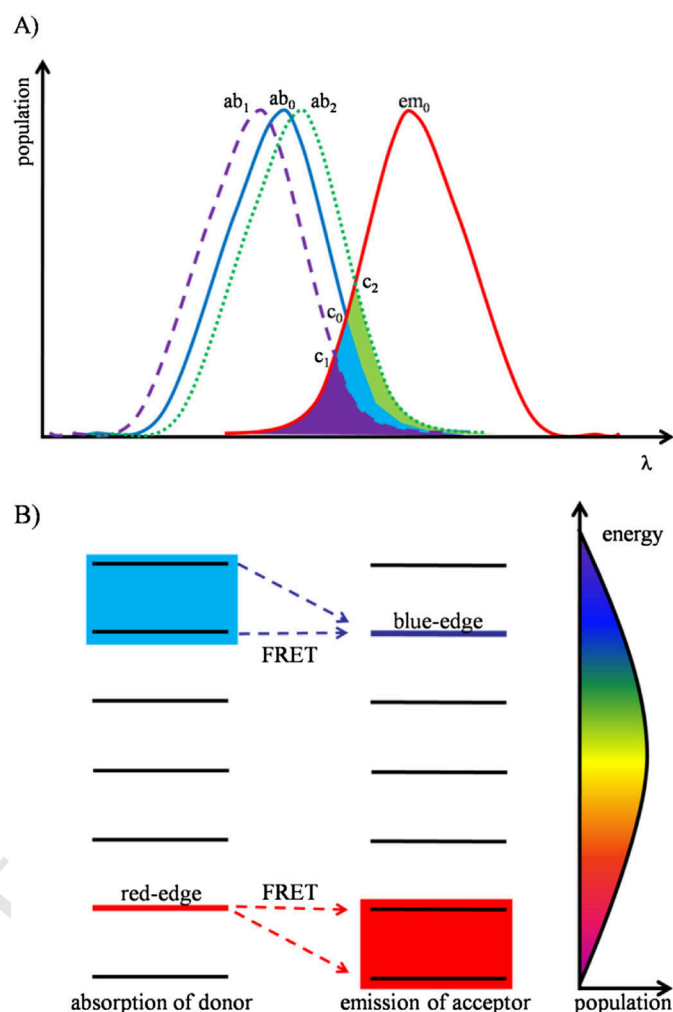


Fig. 1. Cartoons explaining how inhomogeneous broadening induces directed FRET migration. Panel A: Illustration of the mechanism for FRET directionality. A dye with absorption spectrum ab_0 (blue) and emission spectrum em_0 (red) transfers energy with larger probability to dye with absorption spectrum at longer wavelengths like ab_2 (green) than to those with absorption spectrum at shorter wavelengths like ab_1 (violet), due to the larger spectral overlap for FRET. While the overlap between em_0 and ab_2 is larger than the overlap between em_0 and ab_0 with the green portion (with apex c_2), the overlap between em_0 and ab_1 (violet area with apex c_1) is smaller than the overlap between em_0 and ab_0 with the blue portion (with apex c_0). This leads to net energy migration in the direction of decreasing energy levels, like water flows from the hills towards the valleys [16,20]. The emission spectra belonging to absorption spectra ab_1 and ab_2 are not indicated. Panel B: Energy level diagrams for the potential FRET donors (left) and acceptors (right) from an ensemble of a given type of dye. The different solvent microenvironments introduce energetic heterogeneity in the dye population by splitting up a single energy level (the middle one at yellow) into a set of sublevels (3 new levels above and under the middle one). The rainbow-colored contour to the right of the energy ladders represents the population distribution on the energy levels. Directionality in FRET is introduced by the fact that – due to the Stokes-shift, which is not indicated for easiness – overlap integral is larger for those acceptor levels which lie under the donor level from which FRET starts out [16,20] (see also Panel A). A consequence is that FRET predominantly happens towards acceptors of energy levels lower than for the donor leading to a FRET-correlated red shift of the emitted light. For the same reason, the potential acceptor subpopulations for FRET directed from the lower lying donor levels, i.e., at the red-edge, are severely restricted, and manifested in the loss of FRET. Similarly, when selectively monitoring the blue-emitting dyes, i.e., at the emission blue-edge, these species can be potential FRET acceptors only for the very few donors lying upwards in energy, implying a corresponding loss of FRET. Our method is based on an optimal choice of a FRET sensitive (absorption at the main-band and detection at the red) and an insensitive (absorption at the red-edge and detection close to the blue-edge) anisotropy channel. Determination of an absolute homo-FRET efficiency may be possible by the elimination of the dependence on rotation by ratioing the two anisotropies, whenever they have equal sensitivities for the rotation.

147 **2. Materials and methods**148 **2.1. Cell line**

149 The Kit-225-K6 cell line is a human T cell with helper phenotype
150 and with an IL-2 requirement for its growth [25]. Cells were cultured
151 in RPMI-1640 medium supplemented with 10% fetal calf serum, penicil-
152 lin and streptomycin. To the Kit-225-K6 cells 20 U/ml recombinant
153 interleukin-2 (IL-2) was also added in every 48 h.

154 **2.2. Monoclonal antibodies**

155 The production and specificity of monoclonal antibodies (mAbs)
156 applied in the experimental procedures have been described earlier
157 [26,27]. MAbs W6/32 (IgG_{2aκ}) and L368 (IgG_{1κ}) developed against a
158 monomorphic epitope on the α₂, and α₃ domains of the heavy chain
159 and the β₂-microglobulin of MHC I, respectively; mAb L243 (IgG_{2aκ})
160 against MHC II, DRα were kindly provided by Dr. Frances Brodsky
161 (UCSF, CA). Additional mAbs used in spectrofluorimetric measurements
162 were: MEM85 (IgG_{2b}) anti-CD44, and OKT3 (IgG_{2b}) anti-CD3. These
163 mAbs were prepared from supernatants of hybridomas and were puri-
164 fied by affinity chromatography on protein A-Sepharose.

165 **2.3. Preparation of Fab fragments**

166 Fab fragments of the purified antibodies were prepared by papain
167 digestion at an antibody/enzyme (w/w) ratio of 100, at 37 °C for 4–
168 12 h [28]. The digestion products were subjected to ion-exchange chro-
169 matography on DEAE-Sepharose (Pharmacia). The Fab fragments eluted
170 in the flow-through fraction were freed of undigested IgG and of the
171 Fc fragments. Control of the digestion and Fab purification was carried
172 out by SDS/PAGE, enzyme immunoassay, and size-exclusion chroma-
173 tography on Sephacryl S-100 or analytical ultracentrifugation (Beckman
174 Model E).

175 **2.4. Fluorescent staining of antibodies**

176 Aliquots of the proteins for fluorescence conjugation were labeled
177 with 6-(fluorescein-5-carboxamido)hexanoic acid, succinimidyl
178 ester (xFITC) (Molecular Probes, Eugene, OR) or the Alexa-Fluor
179 488 (A488) as the donor (and acceptor) dyes. xFITC has a large ampli-
180 tude tethered motion (segmental mobility) because it contains a
181 7-atom aminohexanoyl spacer (“x”) between the fluorophore and
182 succinimidyl ester moieties. Kits provided with the dyes were used for
183 the conjugation. Detailed labeling procedure of the mAb was described
184 earlier [29,30]. Dye-per-protein labeling ratios for the A488-conjugated
185 whole L243, L368, and W6/32 mAbs (Fabs) were 2.4 (0.47), 3.16 (1.1),
186 and 1.8 (0.85), respectively. Labeling ratios for xFITC-conjugated L243,
187 L368 and W6/32 whole mAbs (Fabs) were 4.9 (1.0), 3.9 (1.95), and
188 3.71 (0.71) respectively. Labeling ratios of additional mAbs used in
189 spectrofluorimetric “free A488-mAb” experiments were: 1.64, 2.41,
190 and 3.92 for W6/32, OKT3, and MEM85 respectively. These values
191 were separately determined for each labeled aliquot in a spectropho-
192 tometer (Hitachi U-2900, NanoDrop ND-1000). The labeled proteins
193 retained their affinity as proven by competition experiments with iden-
194 tical, unlabeled ligands.

195 **2.5. Labeling of cells with mAbs**

196 Freshly harvested cells were washed twice in ice cold PBS (pH 7.4),
197 the cell pellet was suspended in 100 μl of PBS (10⁶ cells/ml) and labeled
198 by incubation with ~10 μg of dye-conjugated mAbs for 40 min on ice in
199 the dark. The excess of mAbs was at least 30-fold above the K_d during
200 incubation. To avoid possible aggregation of the dye-conjugated mAbs,
201 they were air-fused (at 110,000 g, for 30 min) before labeling. Special
202 care was taken to keep the cells at ice cold temperature before FRET

203 measurements in order to avoid unwanted aggregations of cell surface
204 receptors or receptor internalization. Labeled cells were washed twice
205 with ice cold PBS and then fixed with 1% paraformaldehyde. In the titra-
206 tion experiments using the A488-L243, A488-L368, and A488-W6/32
207 mAbs, the final concentrations in μM were 0.6, 0.4, and 0.5, respectively.

208 **2.6. Determination of expression levels of receptors**

209 The relative expression levels of receptors on Kit-225-K6 cells were:
210 MHC I, 100 ± 13.3%; MHC II, 76.6 ± 8.6%, where the 100% level means
211 (1.0–1.5) × 10⁶. The number of binding sites was determined from the
212 mean values of flow-cytometric fluorescence intensity histograms of
213 cells labeled to saturation with the dye-conjugated mAbs (Scatchard-
214 analysis). The mean fluorescence intensities were converted to the num-
215 ber of binding sites by calibration with fluorescent microbeads having
216 known number of fluorescent dyes (Quantum™ Alexa-Fluor 488 MESF,
217 Bangs Laboratories, Inc.). They were also used for the calibration of the
218 forward angle light scattering (FSC) signals in the determination of size
219 of Kit-225-K6 cells, which is 13–14 μm.

220 **2.7. Spectrofluorimetry of labeled cells, free dye and free mAbs**

221 Fluorescence polarized spectra, from which anisotropy spectra were
222 computed, have been recorded with a Fluorolog (Jobin Yvon-Spex)
223 spectrofluorimeter with 5-nm slit widths. In experiments with free
224 dye and free mAbs glycerol (spectroscopic grade, Sigma-Aldrich) has
225 also been added in 33% and 67% volume fractions (v/v) to the free dye
226 or mAbs dispersed in PBS. Spectral recordings have been taken up at
227 room temperature. Anisotropies shown on Fig. 4s in the Supporting
228 information have been computed by averaging anisotropy spectra on
229 the 570–600 nm spectral range.

230 **2.8. Flow cytometric dual-laser dual-anisotropy measurements**

231 Cell-by-cell basis correlated measurements of the polarized intensity
232 components – from which the total intensities and anisotropies are
233 calculated – were carried out in the “dual T-format” arrangement [31]
234 depicted in Fig. 2. It was realized in a modified FACStar^{plus} flow
235 cytometer (Becton-Dickinson) equipped with single-laser excitation
236 facility (Stabilite 2017 Ar⁺-laser, Spectra-Physics Inc. Mountain View,
237 CA, USA), with the laser operating in the “single line” mode set to each
238 of the wavelengths 457.9, 476.5, 488, 496.5 and 514.5 (nm) for record-
239 ing titration plots like the ones in Fig. 3. For measuring absolute homo-
240 FRET efficiency, for which dual-laser excitation is required, the laser was
241 operated in “all lines” mode containing all the above wavelength in
242 a single beam. After introducing into the flow cytometer through a
243 polarization rotator – ensuring determination of the G-factor – the
244 laser beam was deviated with 90° and subsequently split into colors
245 by a Pellin-Broca prism (a kind gift of Prof. Zsolt Bor, Institute of Optics
246 and Optical Engineering, Szeged, Hungary) mounted into the exciting
247 path of the flow cytometer, before reaching the main focusing lens L₁
248 in Fig. 2. The beam-pair for excitation could be chosen at custom with
249 a suitable pair of pinholes cut into a metal sheet and by adjusting the
250 delay-time (30 μs in Fig. 2) between the collected fluorescence signals
251 in the cytometer’s electronic console. The green (FRET-insensitive)
252 and red (FRET-sensitive) components of total fluorescence were separ-
253 ated by an LP 550 dichroic mirror (DM in Fig. 2, manufactured by Ferenc
254 Kárpát at the Central Physics Research Institute, Budapest, Hungary)
255 and subsequently were fed via two band-pass filters (HQ535/25 for sig-
256 nal I₁, and HQ 640/120 for signal I₂, AF Analysentechnik, Tübingen) into
257 two broadband polarization beam splitter cubes (10FC16PB.3, Newport)
258 with green and red sensitive photomultipliers (Hamamatsu) at their
259 output ports defining the 4 polarized intensity channels (I_{1h}, I_{1v}, I_{2h},
260 I_{2v}). For the determination of the G-factor of each fluorescence channel,
261 the originally vertical polarization direction of laser light is rotated
262 by 90° with a Fresnel double rhomb-polarization rotator (Broadband

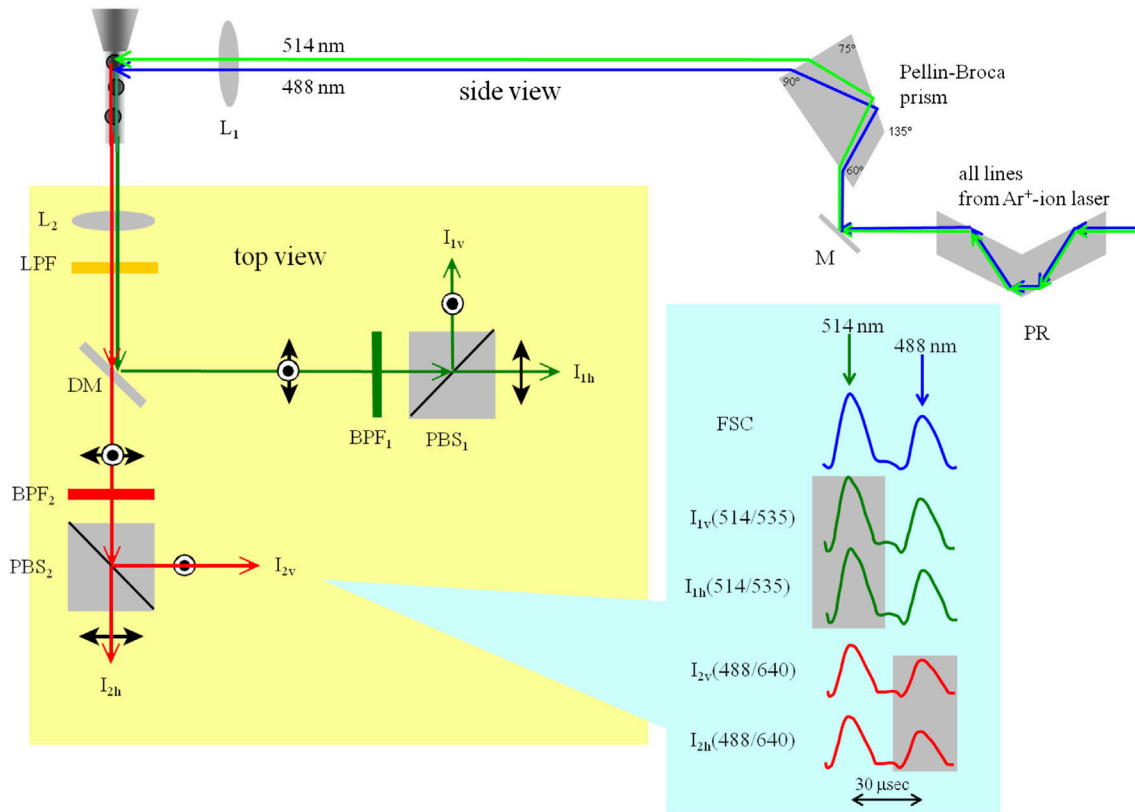


Fig. 2. Optical layout of dual-laser homo-FRET and detected signals. The beam of an Ar⁺-laser in “all lines” mode – only two excitation colors are displayed for convenience – is fed into the cytometer through a “Fresnel double-rhomb” polarization rotator (PR) and a “Pellin-Broca prism” serving for a 90° achromatic beam deflection and beam-separation according to colors. The fluorescence is collected by a lens (L₂), directed after the long-path filter (LPF) by a dichroic mirror beam-splitter (DM) towards the polarization beam-splitter cubes (PBS₁, PBS₂), which together with the respective band-pass filters (BPF₁, BPF₂) realize the “green (1st)” and “red (2nd)” anisotropy channels. “Single-laser line” and “dual-laser line” operations are realized by manual setting the laser resonator for a chosen wavelength, and by cutting the fluorescence spots activated by the unnecessary laser lines by mechanical obscuration (a pair of appropriately positioned pinholes), respectively. In the illustration from the 5 main visible laser lines only the 488 nm- and 514.5 nm-ones are indicated, which realize the main-band and red-edge excitations for the A488 and xFITC dyes.

Polarization Rotator, Model PR-550, Newport) positioned between the laser and the cytometer for both the “single-line” and “all-lines” excitation modes.

2.9. Computation of total intensities and anisotropies

Four polarized intensities have been detected for each signal channel [31,32]: $I_{i,vv}$, $I_{i,vh}$, $I_{i,hv}$, and $I_{i,hh}$, with the first index i designating the signal channel ($i = 1, 2$), the second and third ones referring to the polarization direction of the exciting laser light and that of the fluorescence, respectively (Fig. 2). The signals with the horizontal excitation are detected after the vertical excitation by rotating the polarization direction with 90°. After subtracting the corresponding background intensities measured on the unlabeled cells from the polarized intensities, the correction factors G_i ($i = 1, 2$) balancing the sensitivities of vertical and horizontal fluorescence channels, the total fluorescence intensities I_i , and the fluorescence anisotropies r_i were calculated as follows:

$$G_i = I_{i,hv}/I_{i,hh}, \quad (1)$$

$$I_i = I_{i,vv} + \hat{a}(\psi) \cdot G_i \cdot I_{i,vh}, \quad (2)$$

$$r_i = (I_{i,vv} - G_i \cdot I_{i,vh})/I_i. \quad (3)$$

In the above expression for the total intensities I_i ($i = 1, 2$) a numerical correction for the high aperture fluorescence collection was carried out according to T. M. Jovin [4,32] by using the term $\hat{a}(\psi) \equiv$

$1 + \cos \psi \cdot (1 + \cos \psi)/2$, where $\hat{a}(\psi)$ assumes a value of 1.72 for our numerical aperture of NA = 0.6, and ψ stands for the half angle of the detected light cone. The anisotropy and total intensity values were computed on a cell-by-cell basis from the correlated $I_{i,vv}$ and $I_{i,vh}$ intensities with predetermined values of the G_i factors as input parameters. Based on Eq. (2) the r_{corr} aperture-corrected anisotropy can be written as the function of the r uncorrected one as follows: $r_{\text{corr}} \equiv 3 \cdot r / [1 + \hat{a}(\psi) + r \cdot [2 - \hat{a}(\psi)]]$.

The mean values of fluorescence anisotropy and total intensity histograms measured on the dye-labeled cells ($\sim 10^4$) were further used for the calculation of the absolute homo-FRET efficiencies T_0 , T , and the homo-FRET enhancements η , the most important resulting quantities of the method. The generation and subsequent analysis of flow cytometric histograms (such as those on Figs. 8–10) and 2-dimensional correlation plots (dot-plots) of total fluorescence intensities, fluorescence anisotropies, and homo-FRET efficiencies were performed by a home-made software specialized for flow cytometric data analyses called Reflex, written by G. Szentesi [32], freely downloadable from <http://www.biophys.dote.hu/research.htm>, and <http://www.freewebs.com/cytoflex.htm>.

3. Theoretical results

3.1. Homo-FRET enhancement factors measured on receptor-trimers

If the intensities and anisotropies of samples singly labeled by mAbs {mAb_x, mAb_y, mAb_z} are denoted by I_x , I_y , I_z and r_x , r_y , r_z (Fig. 3, 311

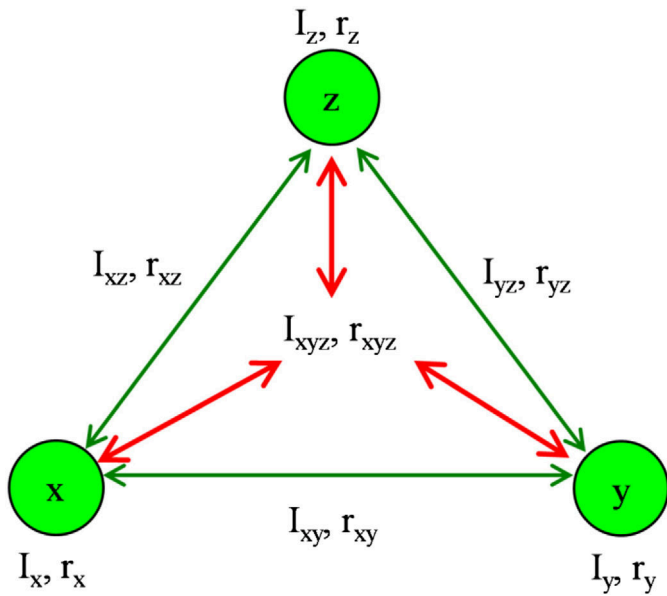


Fig. 3. Cartoon of a receptor trimer with the measured quantities. Logical scheme of homo-FRET measurements in receptor trimers. The encircled numbers designate the receptors with the I_x , I_y , and I_z intensities and r_x , r_y , and r_z anisotropies measurable after singly labeling with the respective mAbs. The I_{xy} , I_{xz} , and I_{yz} intensities and the r_{xy} , r_{xz} , and r_{yz} anisotropies can be measured after pair wise labeling with the respective mAbs. The I_{xyz} intensity and the r_{xyz} anisotropy can be measured after triply labeling with all the mAbs. The homo-FRET enhancement factors η_{xy} , η_{xz} , and η_{yz} are defined in terms of the relative decreases of the pair wise anisotropies as compared to the intensity weighted averages of the respective anisotropies of the singly labeled samples. The homo-FRET enhancement factor η_{xyz} is defined in terms of the relative decrease of the triple anisotropy as compared to the intensity weighted average of the anisotropies of the three singly labeled samples. The differential homo-FRET enhancement factor $d\eta_{xyz}$ is defined in terms of the relative decrease of the triple anisotropy as compared to the intensity weighted average of the pair wise anisotropies of the three doubly labeled samples.

Panel A) then the intensity weighted average of anisotropy for the sample doubly-labeled with mAb_x and mAb_y:

$$\bar{r}_{xy} = (I_x \cdot r_x + I_y \cdot r_y) / (I_x + I_y), \quad (4)$$

with similar equations for \bar{r}_{xz} and \bar{r}_{yz} of the mAb_x–mAb_z, and mAb_y–mAb_z pairs. The intensity weighted average of anisotropy for the sample triply-labeled with mAb_x, mAb_y, and mAb_z can be computed analogously:

$$\bar{r}_{xyz} = (I_x \cdot r_x + I_y \cdot r_y + I_z \cdot r_z) / (I_x + I_y + I_z). \quad (5)$$

For the triply-labeled sample another intensity weighted anisotropy (“grand-average”) can be defined with the intensities I_{xy} , I_{xz} , and I_{yz} and anisotropies r_{xy} , r_{xz} , and r_{yz} of the doubly-labeled samples:

$$\bar{\bar{r}}_{xyz} = (I_{xy} \cdot r_{xy} + I_{xz} \cdot r_{xz} + I_{yz} \cdot r_{yz}) / (I_{xy} + I_{xz} + I_{yz}). \quad (6)$$

Pair-wise homo-FRET enhancement factor (η_{xy}) is defined as the relative decrease of the average anisotropy introduced by the proximity of mAb_x and mAb_y as compared to the average of the respective singly-labeled ones (\bar{r}_{xy}):

$$\eta_{xy} = 1 - r_{xy} / \bar{r}_{xy}, \quad (7)$$

where r_{xy} is the measured anisotropy of the mAb_x–mAb_y – potentially interacting – pair. Triple-wise homo-FRET enhancement factor (η_{xyz})

is defined analogously as the relative decrease of the average anisotropy introduced by the mutual proximity of mAb_x, mAb_y, and mAb_z as compared to the average of the singly-labeled ones (\bar{r}_{xyz}):

$$\eta_{xyz} = 1 - r_{xyz} / \bar{r}_{xyz}, \quad (8)$$

where r_{xyz} is the measured anisotropy of the mAb_x–mAb_y–mAb_z triplet. Differential homo-FRET enhancement factor ($d\eta_{xyz}$) is defined analogously as the relative decrease of the average anisotropy of the triply labeled samples as compared to the average of the doubly-labeled ones ($\bar{\bar{r}}_{xyz}$):

$$d\eta_{xyz} = 1 - r_{xyz} / \bar{\bar{r}}_{xyz}. \quad (9)$$

3.2. Absolute homo-FRET efficiency determination

Because of the possible homo-associations of the different receptor kinds, the initial values of anisotropies may already be influenced by homo-FRET which is not reflected in the above described homo-FRET enhancement values. Absolute homo-FRET efficiencies reflecting both the initial homo-FRET and its enhancement will be defined next, as the ratios of two anisotropies measured in homo-FRET sensitive (r_2) and insensitive (r_1) channels. Our starting point is a factorizing out the two anisotropies in terms of the depolarization factors [22–24] for rotation and FRET ($d_{rot,i}$, $d_{t,i}$ $i = 1, 2$) (Fig. 4) and the zero-time limiting (starting) anisotropy r_0 :

$$r_i = r_0 \cdot d_{rot,i} \cdot d_{t,i}. \quad (10)$$

In Eq. (10) the same r_0 is used for both detection channels, because processes taking place on time scales much shorter than the fluorescence lifetime (e.g., psec-torsional rotations) are responsible for its value. Values of r_0 can be determined in the steady state by recording donor Perrin-plots in the presence of quenching or FRET, or in the time-domain by anisotropy FLIM (rFLIM). As to the geometric meaning,

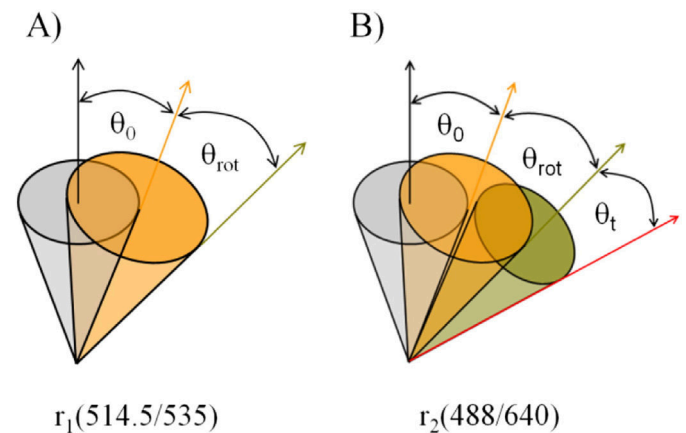


Fig. 4. Cartoon of Soleillet’s cones. Panel A: At red-edge excitation the two factors determining the anisotropy r_1 are the rotations taking place at times scale much shorter than that for fluorescence decay and slower rotations to which orientational cones of θ_0 and θ_{rot} half-cone angles are associated. The quick rotations described by θ_0 determine the initial anisotropy r_0 . The net orientation cone is obtained as the convolution of the cones for the two rotations. Panel B: At the main-band excitation, for anisotropy r_2 , the previous orientation cones should be extended with that for homo-FRET, described by the θ_t half-cone angle. The net orientation cone is obtained as the convolution of the two cones for rotation and that for homo-FRET. Depolarization factors (d_0 , d_{rot} , d_t) can be assigned to the cones, the product of which gives the net depolarization for the case of axial symmetry and independence.

the rotational and FRET depolarization factors can be traced to the half-cone angles θ_{rot} and θ_t in Fig. 4:

$$d_{\text{rot}} = [3 \cdot \cos^2(\theta_{\text{rot}}) - 1]/2, \quad (11)$$

$$d_t = [3 \cdot \cos^2(\theta_t) - 1]/2. \quad (12)$$

After introducing the rotational strengths σ_i defined in terms of the lifetimes τ_i and the $\phi_{\text{rot},i}$ rotational correlation times ($i = 1, 2$) – called also “rotational efficiencies” – as

$$\sigma_i \equiv \tau_i / \phi_{\text{rot},i}, \quad (13)$$

as a 2nd form, the rotational depolarization factors can also be written in terms of the rotational strengths:

$$d_{\text{rot},i} = 1/(1 + \sigma_i). \quad (14)$$

The 2nd form of depolarization factors for homo-FRET is defined analogously, with the A_i ($i = 1, 2$) “normalized rate constants” for homo-FRET:

$$d_{t,i} = 1/(1 + A_i), \quad (15)$$

where A_i is defined as

$$A_i = k_{t,i} \cdot \tau_i. \quad (16)$$

By writing Eq. (10) for 2 arbitrary detection channels (1, 2), it can be seen that in the most general case we have only 2 measured parameters (r_1, r_2) and 5 unknowns: the r_0 limiting anisotropy, supposedly the same for the two channels, the $\tau_1/\phi_{\text{rot},1}$ and $\tau_2/\phi_{\text{rot},2}$ “normalized rotational rates” (“rotational efficiencies”), and the A_1 and A_2 “normalized homo-FRET rate constants” in the two channels. In contrast to the identity of the r_0 limiting anisotropy in the two channels, these latter quantities are supposedly different from each other because the two channels represent different photoselected microenvironments of the fluorophores characterized by different strengths of interactions. To proceed, however, we assume that both the ratio of the normalized rotational rates and the ratio of homo-FRET rates are constants known from previous calibrations or assumptions, e.g., an assumption on the level of residual homo-FRET in the homo-FRET insensitive channel. We introduce the spectral correction factor β taking into account the difference in the σ_i ($i = 1, 2$) “rotation strengths”

$$\beta \equiv (1 + \sigma_2)/(1 + \sigma_1), \quad (17)$$

and the γ factor comparing the homo-FRET levels in the two channels

$$\gamma \equiv A_1/A_2. \quad (18)$$

By comparing Eq. (16) for β with Eq. (13) we can see that β can also be expressed with the rotational depolarization factors ($d_{\text{rot},i}$, $i = 1, 2$) as follows:

$$\beta = d_{\text{rot},1}/d_{\text{rot},2}. \quad (19)$$

By using Förster's formula connecting the FRET rate constant and lifetime product – i.e., A_i according to Eq. (16) – to the characteristic Förster distances $R_{0,i}$ and the inter-chromophore distance R , written for signal channel i as:

$$A_i = (R_{0,i}/R)^6, \quad (20)$$

γ can be expressed with the ratio of the R_0 -s for the two channels:

$$\gamma = (R_{0,1}/R_{0,2})^6. \quad (21)$$

By assuming known values of the β and γ spectral corrections, and using the definition of the homo-FRET efficiency in channel 2, designated as T ,

$$T = A_2/(1 + A_2), \quad (22)$$

after taking the ratio (r_2/r_1) of the two anisotropies factorized according to Eq. (10), T can be expressed with the correction factors and the anisotropy ratio as follows:

$$T = (1 - \beta \cdot r_2/r_1)/(1 - \gamma). \quad (23)$$

By introducing the uncorrected homo-FRET efficiency T_0 obtainable from Eq. (22) for the ideal case of identical rotational strengths in the two channels ($\beta = 1$) and complete absence of homo-FRET ($\gamma = 0$) in the homo-FRET insensitive channel,

$$T_0 = 1 - r_2/r_1, \quad (24)$$

T can be cast in the alternative forms as expressions of β , γ , and T :

$$T = [T_0 \cdot \gamma + (1 - T_0) \cdot (1 - \beta)]/(1 - \gamma) + T_0, \quad (25)$$

$$T = [(1 - \beta) + \beta \cdot T_0]/(1 - \gamma). \quad (26)$$

By inspecting Eqs. (23), and (25) the correction factors β and γ always increase the value of the homo-FRET efficiency – i.e., $T > T_0$ – whenever the $\beta < 1$ and $\gamma > 0$ relations hold. Because complete lack of homo-FRET in the insensitive channel cannot be guaranteed, small positive values can be expected for γ expressing the degree of residual homo-FRET. As to β , because in the FRET insensitive channel the fluorophore–environment interactions are expected to be larger than in the FRET sensitive channel, implying also smaller lifetime and larger rotational correlation time in this channel, the validity of the $\beta < 1$ relation can be expected on the basis of Eq. (17).

After expressing the absolute homo-FRET efficiencies T_1 and T_2 ($T_2 = T$) with the corresponding A_i parameters similarly to Eq. (21), the FRET depolarization factors $d_{t,i}$ can be expressed in terms of T_i :

$$d_{t,i} = 1 - T_i. \quad (27)$$

In the 1st detection channel when $T_1 = 0$ – i.e., $d_{t,1} = 1$ according to Eq. (26) – in the knowledge of r_0 the rotational depolarization factor $d_{\text{rot},1}$ can be expressed from Eq. (10) (written for $i = 1$) as:

$$d_{\text{rot},1} = r_1/r_0, \quad (28)$$

which can be solved for the rotational correlation time $\phi_{\text{rot},1}$ in the knowledge of τ_1 (Eqs. (13), (14)). Alternatively, by considering the 2nd detection channel in Eq. (10), $d_{\text{rot},2}$ can also be expressed in a similar way with the known parameters r_0 and T_2 ($T_2 = T$):

$$d_{\text{rot},2} = r_2/[r_0 \cdot (1 - T)], \quad (29)$$

where Eq. (27) was also used for expressing $d_{2,t}$ in terms of T .

3.3. Calibration of homo-FRET efficiency

The β and γ spectral correction factors can be determined by recording fluorescence anisotropy as the function of changing fluorophore concentration, i.e., via recording homo-FRET titration Perrin-plots. On the cell surface this condition can be realized by applying a gradually increasing concentration series of the labeling mAbs. After plotting

the reciprocal anisotropy as the function of degree of saturation p – probability of receptor occupation, the fraction of binding sites occupied by ligands –, defined as the fluorescence intensity referenced to that at saturation, i.e., $p \equiv I(c)/I_{\max}$, a fairly linear curve results, the linear fitting of which makes possible the separation of the effects of rotational motion and homo-FRET on anisotropy. The point of this procedure is in that it effectively eliminates the need for negative control sample of zero homo-FRET, because by gradually decreasing the cell surface concentration of the fluorophores the zero homo-FRET condition is realized at the limiting case when $c \rightarrow 0$ even if the labeling ratio of ligand is larger than unity, i.e., the need for a zero-FRET negative control is replaced by a limiting procedure.

The analytical form of the fitting function can be obtained by taking the reciprocal of the anisotropy as factorized out according to Eq. (10) [4,34], by also taking into account the definitions of the d_{rot} and d_t depolarization factors formulated in Eqs. (14), and (15):

$$1/r(p) = 1/r' + (1/r') \cdot A \cdot p, \quad (30)$$

where r' – meaning the homo-FRET free anisotropy – has been defined as

$$r' \equiv r_0/(1 + \sigma). \quad (31)$$

According to Eq. (30) r' can be obtained as the reciprocal intercept (1/intercept) and A as the ratio of the slope and intercept (slope/intercept) of the fitting straight line. By carrying out this procedure in both the FRET sensitive (2nd) and insensitive (1st) channels the β and γ factors can be obtained as the ratios of the corresponding r' and A quantities, respectively, according to the defining Eqs. (17), and (18). Although the maximum local fluorophore concentration dictated by the receptor number and the labeling ratio and other factors are involved in the A quantity for each mAb, it drops out from γ because of ratioing, consequently γ depends only on the fluorophore properties.

3.4. Connection between homo-FRET enhancement and absolute efficiency

The main use of the homo-FRET enhancement factors lies in that they can be regarded as a clear measure of the degree of proximity of neighboring receptors because by ratioing the depolarizing effects of rotation and homo-FRET on the individual ligands cancel in the formulae, albeit reducing sensitivity to the receptor proximities. Only the differential homo-FRET effect due to the receptor proximity remains. Amongst the factors limiting their application is that in cases of multiple receptor labeling chance for quenching by dim dye complexes increases, consequently the fluorescence lifetime reduces and the induced hyperpolarization partly counteracts the depolarizing effect of homo-FRET. Another limit can arise at large dye-per-ligand labeling ratios, when the depolarizing effect of homo-FRET may effectively be restricted to the ligand itself (“homo-FRET confinement”) thereby reducing sensitivity to the receptor proximities.

In contrast to the homo-FRET enhancements, homo-FRET efficiency reflects homo-FRET between receptors and also on the individual ligands. Nevertheless, FRET efficiency enhancements can also be formed similarly to the above homo-FRET enhancements (percentile anisotropy reductions). Differential FRET efficiency (δT) can be defined as an absolute increase in FRET efficiency due to the proximity of two (or more) receptors, and measured as the absolute difference between the FRET efficiency measured on the multiply labeled (labeled with both mAb_x and mAb_y) sample (T_{xy}) and the intensity weighted average efficiency of the singly labeled ones (\bar{T}), labeled with either mAb_x or mAb_y labels (\bar{T}):

$$\delta T \equiv T_{xy} - \bar{T}, \quad (32)$$

where T_{xy} and \bar{T} are written as

$$T_{xy} = 1 - r_{2,xy}/r_{1,xy}, \quad (33)$$

$$\bar{T} = (I_{1,x} \cdot T_x + I_{1,y} \cdot T_y) / (I_{1,x} + I_{1,y}). \quad (34)$$

(Although these FRET efficiencies are not corrected with β and γ , from here on in this section the subscript zero indicating this fact is neglected for the sake of transparency. Additionally all results of this section remain valid also for the corrected FRET efficiencies.)

First, by introducing the homo-FRET enhancements η_i for channel i ($i = 1, 2$) according to Eq. (7),

$$\eta_i \equiv 1 - r_{i,xy}/\bar{r}_i, \quad (35)$$

with $r_{i,xy}$ the anisotropy of the sample doubly labeled with both species x and y , and the average anisotropy \bar{r}_i defined as

$$\bar{r}_i \equiv (r_{i,x} \cdot I_{i,x} + r_{i,y} \cdot I_{i,y}) / (I_{i,x} + I_{i,y}), \quad (36)$$

and by eliminating $r_{i,xy}$ ($i = 1, 2$) in Eq. (33) for T_{xy} with the help of Eq. (35), T_{xy} assumes the form

$$T_{xy} = 1 - \bar{r}_2/\bar{r}_1 \cdot (1 - \eta_2)/(1 - \eta_1). \quad (37)$$

Then, by writing the individual FRET efficiencies T_x and T_y in terms of anisotropies according to Eq. (24) as

$$T_x = 1 - r_{2,x}/r_{1,x}, \quad (38)$$

and

$$T_y = 1 - r_{2,y}/r_{1,y}, \quad (39)$$

Eq. (34) transforms into

$$\bar{T} = 1 - \bar{r}_2/\bar{r}_1. \quad (40)$$

After plugging the expressions of Eq. (37) and Eq. (40) for T_{xy} and \bar{T} into Eq. (32), by exploiting the approximation that the “inner average” equals “outer average”, i.e.,

$$\bar{r}_2/\bar{r}_1 \approx r_{2,xy}/r_{1,xy}, \quad (41)$$

and by exchanging \bar{r}_2/\bar{r}_1 with \bar{T} via Eq. (40), δT translates into its final form readily amenable for interpretation:

$$\delta T \approx (1 - \bar{T}) \cdot (\eta_2 - \eta_1) / (1 - \eta_1). \quad (42)$$

According to Eq. (42) the differential FRET efficiency δT approximates well the difference in the homo-FRET enhancements for small average FRET efficiencies ($\bar{T} \approx 0$) and small homo-FRET enhancements ($\eta_1 \approx 0$) in the insensitive channel.

4. Experimental results

4.1. Dispersion of homo-FRET titration curves

4.1.1. Qualitative description: operation of red-edge effects on the cell surface

Because the red-edge effects were originally discovered for systems of high rigidity and viscosity (colored plastics, glasses), the main concern for a possible application refers to the mere existence of these effects in the highly mobile systems of fluorophores targeted by mAbs to cell surface receptors. As a 1st type of experiment, homo-FRET was

modulated by systematically changing the amount of fluorophore-conjugated mAbs bound to the MHCI and MHCII receptors – key receptors of adaptive immunity responsible for the presentation of foreign antigens on the infected target cells to the T-cell receptors (TcRs) of the killing and helper cells – having a substantial degree of homo-association [4,21]. Apart from demonstrating the red edge effects on the cell surface, these measurements have also been utilized for calibration purposes, to determine the β and γ correction factors (Eqs. (17), (19)) necessary for the accurate determination of absolute homo-FRET efficiency T .

Anisotropies of fluorescence excited with the visible lines of the Ar⁺-ion laser were simultaneously measured at the green (535/35, mean/width of transmission in nm) and red (640/120) emission channels (r_1 , r_2) in the flow cytometer (Fig. 5, Panels A, B). The following features of the data are notable: (i) Both the green (r_1) and red (r_2) anisotropies substantially decrease with increasing concentration of the label at excitation wavelengths smaller than the excitation maximum (457.9, 476.5 and 488 nm) with the largest effect observed at 457.9 nm, indicating the operation of homo-FRET at these excitations. (ii) A remarkably

smaller degree of drop was observed at the excitation maximum 496.5 nm and no drop at all was observed at 514.5 nm, close to the red-edge. (iii) The intensity ratios I_2/I_1 increase in parallel with the drop of the corresponding r_2/r_1 curves (Fig. 5, Panels C, D) indicating a red shift in the emission spectrum proportional to the degree of homo-FRET. (iv) Although the starting values of the green and red anisotropies are practically the same, red anisotropies drop more steeply than the green ones, implying that sensitivity of the red anisotropy for homo-FRET is larger than that of the green one. That red anisotropy is more sensitive to homo-FRET than the green anisotropy is also shown by that the r_2/r_1 ratio drops with increasing surface concentration of the fluorophore (Fig. 5, Panel D).

In addition to the I_2/I_1 total intensity ratio, the $[I_2/I_1]_{rel}$ and the $[I_{2vh}/I_{1vh}]_{rel}$ quantities – analogues of logarithmic derivatives – (Fig. 5, Panels E, F) were also computed. $[I_2/I_1]_{rel}$ refers to I_2/I_1 ratios normalized to that special I_2/I_1 ratio belonging to the smallest fluorophore concentration. $[I_{2vh}/I_{1vh}]_{rel}$ designates an analogue quantity but computed from the horizontally polarized intensity components instead of the total intensities. This quantity is a more sensitive indicator of homo-

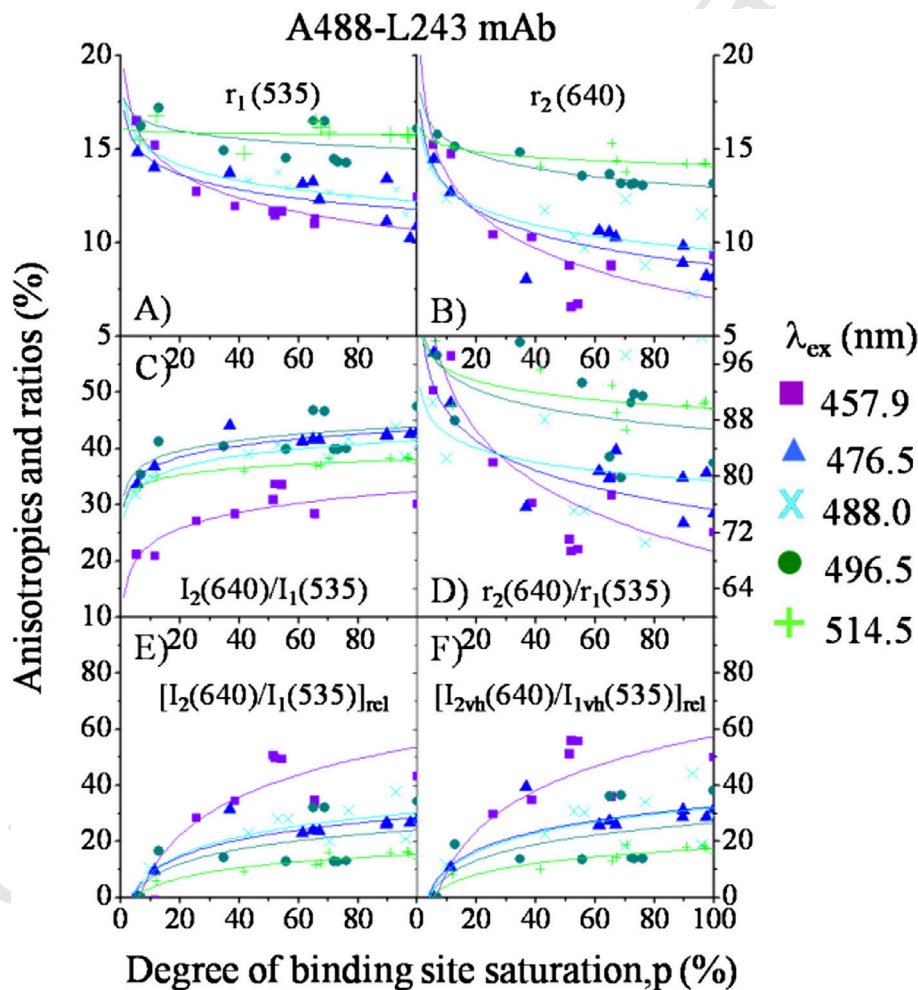


Fig. 5. Dispersion of homo-FRET titration curves according to the color of exciting light. Panels A, B: Drop of anisotropy r_1 and r_2 with increasing degree of saturation of the receptor MHCII labeled with the dye-conjugated mAb L243 for the main lines of the Ar⁺-laser. "Degree of binding site saturation" has been defined as the ratio of fluorescence intensity measured at the given mAb concentration and the plateau value obtained at saturation. Values 535 and 640 refer to the detected 535 ± 17.5 and 640 ± 60 bands. Panels C, D: Relative intensities (I_2/I_1) and relative anisotropies (r_2/r_1) as functions of the relative saturation. Panels E, F: $[I_2/I_1]_{rel}$ refers to the I_2/I_1 ratio normalized to the value belonging to the smallest fluorophore concentration, $[I_{2vh}/I_{1vh}]_{rel}$ designates an analogue quantity but computed from the horizontally polarized intensity components instead of the total intensity (with the excitation and emission wavelengths in parantheses). This quantity is a more sensitive indicator of homo-FRET than either the pure I_2/I_1 or the r_2/r_1 ratio alone, the anisotropy and total intensity being contained in such a manner that the effects of reducing anisotropy and increasing I_2/I_1 ratio add together: $I_{vh} \propto (1 - r) \cdot I_{tot}$. The curves report that homo-FRET can be more sensitively detected in the red channel than in the green one. Furthermore, excitations below 476.5 nm are more favorable for FRET than above it. Absolute homo-FRET efficiency can be calculated the most accurately in the 488/640, and 514.5/535 measuring conditions, which are the most and the least sensitive to homo-FRET. Trend lines are drawn for guiding the eye. Means of 3 determinations are plotted with SEM under 10% for each data point (not indicated).

584 FRET than either the I_2/I_1 or the r_2/r_1 ratio alone, the anisotropy and total
585 intensity being contained in such a manner that the effects of reducing
586 anisotropy and increasing I_2/I_1 ratio add together.

587 As a summary, homo-FRET monotonously decreases with increasing
588 excitation wavelength and is effectively cut at already the excitation
589 maximum. These observations imply the strong modulation of overlap
590 integral with the changing excitation wavelength, which suggests a
591 slow relaxation of the excited state. The slow relaxation rate is also im-
592 plied by a value of 0.4 for the lifetime-per-rotational correlation time
593 ratio (τ/ϕ_{rot}) observed by us earlier [32] and now by rFLIM (see in the
594 Supporting information). A quantitative comparison of the I_2/I_1 ratios
595 as the function of excitation wavelength demands a correction to the
596 different sensitivities of the detection channels (“ α -factor”) belonging
597 to the different wavelengths [36].

598 **4.1.2. Quantitative description: determination of correction factors for**
599 **homo-FRET**

600 For a more quantitative description of the above properties of the
601 titration curves, least-squares linear fitting analyses – detailed in the
602 “Supporting information” – of the reciprocal anisotropy vs. degree of
603 binding site saturation curves plotted from anisotropy data of Fig. 5
604 for the MHCII receptor, and pertinent data on the light and heavy
605 chain components of the MHCI receptor (not shown) has also been
606 carried out to determine the β and γ correction factors in the spirit of
607 Eq. (30). The outcomes of the linear fitting procedure carried
608 out for each excitation wavelength – 457.9, 476.5, 488, 496.5 and
609 514.5 (nm) – are the homo-FRET free anisotropy (r') reflecting only
610 rotation and the A quantity describing the strength of homo-FRET
611 [4,34]. By inspecting the relevant figure composed from these data it
612 can be that: (i) While the homo-FRET-related quantity A increases
613 with reducing excitation wavelength for all the three receptors in both
614 emission channels, the slope of increase is much larger for the red
615 than for the green channel. (ii) The slopes of increase of A are approxi-
616 mately the same for the different types of receptors indicating that the
617 wavelength dependence of the A parameter is characteristic to the
618 fluorophore rather than to the receptors. (iii) As to the wavelength de-
619 pendence of the anisotropy r' , apart from the statistical fluctuation it

620 stays constant at the same level for both the green and red channels
621 for each receptor. The variability regarding receptor type is supposedly
622 due to different segmental flexibilities of the dye.

623 To reduce measurement error the computation of the β factor
624 has been carried out with r'_i values averaged over all wavelengths
625 ($\beta = r'_i/r'_j$, Eq. (17)). For the same reason, and because the wavelength
626 dependence of A turned to be fairly linear, the determination of the γ
627 factor have been carried out with the corresponding A values read
628 off from the fitting trend lines – 514.5 nm in the green for A_1 , and
629 488 nm in the red for A_2 – instead of the primarily observed data points
630 ($\gamma = A_2/A_1$, Eq. (18)). The resulting correction factors, which have been
631 subsequently used for the computation of T and δT in Tables 1, 1s and 2s,
632 are the following (in the form $\beta(\%)/\gamma(\%)$ for type mAb, each from 3 pairs
633 of titration plots): $100.0 \pm 12/5.8 \pm 12.0$ for L243, $94.5 \pm 2.5/7.3 \pm 1.2$
634 for L368, and $96.0 \pm 15.4/13.0 \pm 2.9$ for W6/32.

635 **4.2. Homo-FRET enhancement factors for receptor trimers**

636 In our 2nd type of experiments for demonstrating the red-edge
637 effects, components of a receptor trimer in close proximity were labeled
638 individually and simultaneously with the fluorophore-conjugated
639 ligands (whole mAbs and their Fab fragments). The advantage of this
640 kind of a homo-FRET system lies in its inherently large signal-to-noise
641 ratio and in the possibility for a rather straightforward quantitation of
642 homo-FRET. Pair wise (triple wise) homo-FRET enhancement factors
643 η_{xy} , η_{xz} , and η_{yz} (η_{xyz}) are defined as the relative decrease of anisotropy
644 of the doubly (triple) labeled samples r_{xy} , r_{xz} , and r_{yz} (r_{xyz}) compared
645 with the intensity weighted average of the corresponding single-
646 labeled ones \bar{r}_{xy} , \bar{r}_{xz} , and \bar{r}_{yz} (\bar{r}_{xyz}) (Eqs. (4)–(9), Fig. 3). These quantities
647 differ from zero only when the mutual proximity of two (three) differ-
648 ent types of receptors enables new extra pathways for the homo-FRET
649 between the fluorophores of the different labels. Remarkable is that,
650 because of the ratiating, the effect of a possible rotational motion drops
651 out, and the homo-FRET enhancement values reflect real homo-FRET
652 changes. Differential homo-FRET enhancement ($\delta\eta_{xyz}$) is defined by
653 comparing the anisotropy of the triply labeled sample (r_{xyz}) with the

t1.1 **Table 1**

t1.2 Fluorescence anisotropies (r_1 , r_2), homo-FRET enhancements (η_1 , η_2) and anisotropy ratio-based absolute homo-FRET efficiency (T) for the MHCII- β_2 m-MHCI h.c. receptor trimer labeled
t1.3 with A488-conjugated mAbs on the surface of Kit-225-K6 cells.

Alexa Fluor-488-conjugated whole mAbs						Spectral correction factors (%)		Anisotropies (%)		Homo-FRET parameters					
										Enhancements (%)		Efficiency (%)			
												Uncorrected		Corrected	
mAb _x ^a	Epitope _x	mAb _y ^a	Epitope _y	mAb _z ^a	Epitope _z	β^b	γ^b	r_1^c	r_2^c	η_1^d	η_2^d	T_0^e	δT_0^e	T^f	δT^f
<i>Part A, single-labeled</i>															
L243	MHCII, DR α	–	–	–	–	100.0	5.8	13.9 ± 0.5^g	11.9 ± 0.5	–	–	12.4 ± 3.8	–	13.2 ± 4.1	–
–	–	L368	β_2 m	–	–	94.5	7.3	15.5 ± 0.5	13.9 ± 0.5	–	–	9.9 ± 1.1	–	16.1 ± 1.1	–
–	–	–	–	W6/32	MHCI, h.c.	96.0	13.0	15.9 ± 1.3	14.2 ± 1.5	–	–	10.4 ± 2.4	–	16.1 ± 2.7	–
<i>Part B, double-labeled</i>															
L243	MHCII, DR α	L368	β_2 m	–	–	98.0	6.4	14.9 ± 0.1	12.1 ± 0.1	-2.7 ± 1.4	5.5 ± 1.4	18.8 ± 0.1	7.3 ± 2.8	21.9 ± 0.2	7.7 ± 3.0
L243	MHCII, DR α	–	–	W6/32	MHCI, h.c.	98.5	8.6	15.1 ± 0.3	12.1 ± 0.7	-3.4 ± 4.3	6.4 ± 1.1	20.2 ± 3.0	8.3 ± 4.6	23.4 ± 3.5	8.8 ± 4.9
–	–	L368	β_2 m	W6/32	MHCI, h.c.	95.0	10.1	15.6 ± 0.8	13.1 ± 0.6	-0.1 ± 2.6	6.1 ± 1.6	15.9 ± 0.2	5.5 ± 0.8	22.1 ± 0.2	5.8 ± 0.9
<i>Part C, triple-labeled</i>															
L243	MHCII, DR α	L368	β_2 m	W6/32	MHCI, h.c.	97.0	8.2	15.5 ± 0.4	12.1 ± 0.5	-4.3 ± 0.9	7.9 ± 2.1	21.9 ± 1.5	10.6 ± 2.9	26.2 ± 1.7	11.1 ± 3.0

t1.20 The values designate averages and their associated standard errors (SEM) for 3 measurements.

t1.21 ^a Dye/protein labeling ratios of the mAbs: $L_{A488-L243-mAb} = 2.4$, $L_{A488-L368-mAb} = 3.16$, $L_{A488-W6/32-mAb} = 1.8$.

t1.22 ^b Correction factors have been determined according to Eqs. (17), (18), (30), and (31) for each mAb. Correction factors for the mAb_i-mAb_j pairs (i, j = x, y, z) and the mAb_x-mAb_y-mAb_z triplet are intensity weighted averages of the factors for the corresponding individual mAbs.

t1.23 ^c Anisotropies r_1 and r_2 have been measured in the homo-FRET insensitive (514.5 nm-excitation, 535 nm emission) and sensitive (488 nm-excitation, 640 nm emission) channels, respectively.

t1.24 ^d Homo-FRET efficiency enhancements η_1 and η_2 have been computed as relative anisotropy reductions due to the introduction of a 2nd label as compared to the intensity weighted average anisotropy of the corresponding single-labeled samples (Eqs. (7), (8)).

t1.25 ^e Absolute homo-FRET efficiency T_0 was computed as the relative difference between the homo-FRET sensitive (r_2) and insensitive (r_1) anisotropy: $T_0 \equiv 1 - r_2/r_1$. δT_0 means the absolute difference between the homo-FRET efficiency of the multiply (doubly or triply) labeled samples and the intensity weighted average for the corresponding singly-labeled samples.

t1.26 ^f Spectral corrections have been made according to Eq. (23).

intensity weighted average of the doubly labeled ones (\bar{r}_{xyz}). This value is different from zero whenever triplets of the receptors are present. Because the possible homo-associations of the different receptor kinds, the initial values of anisotropies can already be influenced by homo-FRET which is not reflected in the aforementioned homo-FRET enhancement values. Absolute homo-FRET efficiencies reflecting both the initial homo-FRET and its enhancement will be defined later, via the ratio of two anisotropies measured in different emission channels, in a favorable one, and in an unfavorable one for FRET.

4.3. Dispersion of homo-FRET in A488-mAb trimers

Pair wise and triple wise homo-FRET were measured in the system comprised of the light and heavy chains of the MHC I molecule (L368 anti- β_2m , W6/32 anti-MHCI h.c.) and the MHC II molecule (L243 anti-DR α). The same signals were detected as for recording the homo-FRET titration curves above. Inspecting the data (Fig. 6), the following statements can be made: (i) The red anisotropies (r_2) are all systematically smaller than the corresponding green ones (r_1), and show a larger degree of modulation concerning both excitation wavelengths and the number of labels (Fig. 6, Panels A, B). When their dependence on excitation wavelength is considered they both show a systematic increase with increasing excitation wavelength. (ii) Accordingly, the homo-FRET enhancement factors calculated from the red anisotropies are all larger than those calculated from the green ones (Fig. 6, Panels C, D). Additionally both enhancement factors increase steadily with reducing the excitation wavelength, in accordance with a larger degree of modulation of the anisotropies as the function of the number of labels at the shorter wavelengths. (iii) The I_2/I_1 ratio is increased by increasing the number of the applied mAbs in a degree larger at the shorter wavelengths (Fig. 6, Panel E). (iv) The behavior of the r_2/r_1 ratio is consistent with the behavior of the r_2 and r_1 anisotropies (Fig. 6, Panel F): With increasing excitation wavelength the r_2/r_1 ratio increases, meanwhile showing less modulation at the larger wavelengths when the number of labels is considered. Pertinent data on A488-Fab trimers and xFITC-mAb trimers are shown in Figs. 1s, and 2s in the Supporting information.

4.4. Spectrofluorimetric detection of red-edge effects

4.4.1. Fluorescence spectra recorded on cells triple-labeled with A488-mAbs conform the presence of red-edge effects

According to Fig. 7, Panel A, practically no difference can be seen between the peak positions of emission spectra $I(\lambda)$ recorded at excitation wavelengths under 505 nm. However the significant shift of 6–7 nm in emission spectrum observed at 514 nm-excitation suggests that a substantial degree of static inhomogeneous broadening should be behind the observed red-edge effects. Anisotropy spectrum $r(\lambda)$ seems to be more sensitive to the excitation wavelength than the emission spectrum $I(\lambda)$ (Panel B), the anisotropy spectrum being substantially enhanced already at the 505 nm-excitation. This observation is in good line with also the flow cytometric observations when the r_2/r_1 anisotropy ratio was more significantly modulated by the changing excitation wavelength than the I_2/I_1 intensity ratio (Figs. 5, 6, 1s, 2s). The remarkable decrease in $r(\lambda)$ anisotropy spectrum with increasing emission wavelength suggests the operation of the blue-edge effect. Also this decrease seems to be larger at the shorter excitation wavelengths when homo-FRET is favored. On Panels C and D spectra are shown after division with those recorded at 514.5 nm. Pertinent spectra recorded for the xFITC-mAb trimer are shown in Fig. 3s in the Supporting information.

4.4.2. Red-edge effects on free dyes and free mAbs

Additional control measurements have been carried out with a spectrofluorimeter in free solution condition in cuvettes on A488 dyes and A488-conjugated mAbs having different dye-per-protein labeling ratios in the presence of different amounts of glycerol to modify rotational mobility. On free dyes in a concentration not enough to show any homo-FRET although the zero anisotropies measured at 488 and 514 excitation wavelengths in the absence of glycerol turned into successively larger ones with increasing amount of glycerol, they remained equal with each other, indicating the absence of any homo-FRET also in the presence of glycerol. However on free mAbs added in amounts to reproduce the bulk dye concentration of the free dye solution finite albeit small anisotropies have been observed even in the absence of glycerol

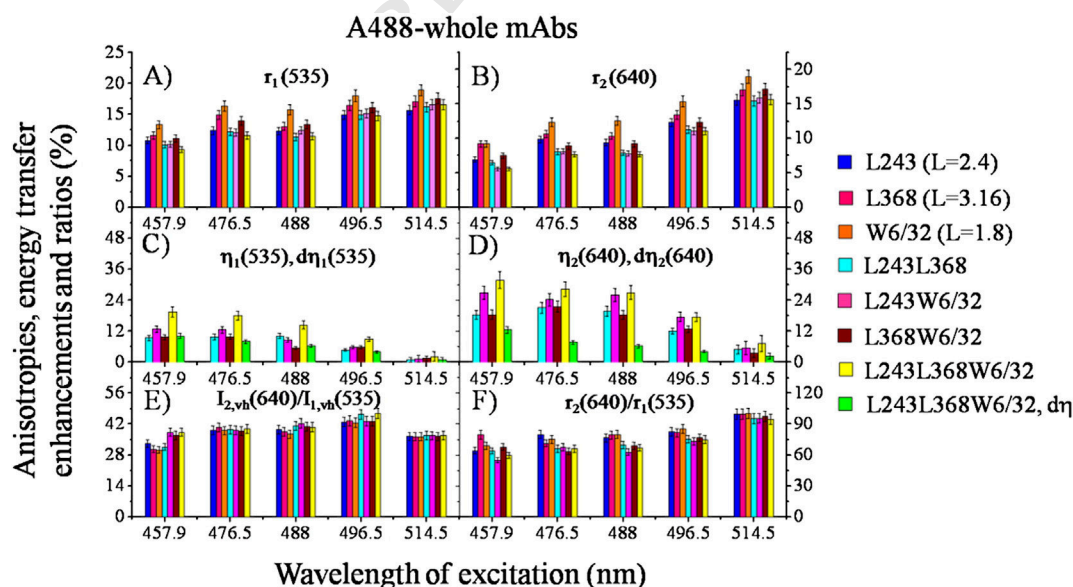


Fig. 6. Dispersion of homo-FRET in A488-mAb trimers. Pair-wise and triple-wise homo-FRET were measured in the system comprised of the light and heavy chains of the MHC I molecule (L368, W6/32 whole mAbs) and the MHC II molecule (L243 mAb). L designates the dye-per-protein labeling ratio of the mAbs. The same signals were detected as for recording the homo-FRET titration curves of Fig. 1. Panels A, B: r_1 and r_2 are the anisotropies detected in the green and red channels. Panels C, D: The corresponding pair-wise homo-FRET enhancement factors are η_1 , and η_2 . The differential enhancement factors are $d\eta_1$, and $d\eta_2$. Panels E, F: Ratios of total intensities (I_2/I_1) and of anisotropies (r_2/r_1). Note that the I_2/I_1 intensity ratio goes through a maximum at 488 nm. Absolute homo-FRET efficiency can be calculated the most accurately in the 488/640, and 514.5/535 measuring conditions, which are the most and the least sensitive to homo-FRET, respectively. Means of 3 determinations are plotted with error bars indicating SEM for each data point. Pertinent data on A488-Fabs, and xFITC-mAbs are shown in Fig. 1s, and 2s in the Supporting information.

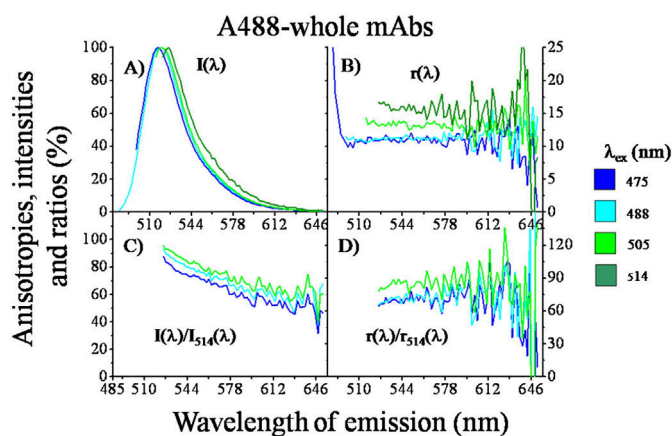


Fig. 7. Fluorimetric spectral recordings on samples triple-labeled with A488-mAbs. Panels A, B: Emission and anisotropy spectra ($I(\lambda)$, $r(\lambda)$) parameterized with the excitation wavelength (with a 5-nm slit width). The significant shift of 6–7 nm in emission spectrum observed at 514 nm-excitation suggests that a substantial degree of static inhomogeneous broadening should be behind the observed red-edge effects. Panels C, D: Spectra normalized to those at 514-nm excitation. Pertinent spectra for xFITC-mAbs are shown in Fig. 3s of the Supporting information.

which showed also a dependence on excitation wavelength. By increasing the amount of glycerol, although the anisotropies steadily increased, the difference experienced at the two excitations reduced. An interesting observation, which is also another indication of the presence of homo-FRET, is that while the absolute anisotropies showed a steady decrease with increasing labeling ratio of the mAbs their relative differences with respect to the excitation wavelength – the FRET-related $[1 - r_2(488)/r_1(514)]$ quantity – showed an increase.

These results indicate that nano-scale clustering of dyes at the same bulk concentration where no homo-FRET were observed on free dyes gave rise to homo-FRET which manifested itself an excitation wavelength and labeling ratio-dependent homo-FRET. That the difference of anisotropies measured at the two wavelengths decreased with increasing amount of glycerol we explain with a decreased strength of homo-FRET due to the decreased rotational mobility and consequently a decrease in orientation factor for FRET. On the details of these experiments and data please see the Supporting information.

4.5. Computation of absolute homo-FRET efficiency

The depolarizing effects of rotation and homo-FRET were separated by applying Soleillet's orientation cones and the associated depolarization factors (Fig. 4, Panel B, Eqs. (10)–(29)). The anisotropy can be written as the product of the initial anisotropy (r_0) and the depolarization factors (d_{rot} , d_t) taking into account the different interactions leading to depolarization of anisotropy (Soleillet's theorem) [22–24]. The formalism is strictly valid only for isotropic and independent interactions, and for axially symmetric orientation distributions. Absolute homo-FRET efficiencies (T_0 , T) were computed based on the Soleillet's theorem. In the ideal and simplest case when the r_0 limiting anisotropy and the τ/ϕ_{rot} ratio is at least approximately the same in the two detection channels, furthermore the extent of homo-FRET in the red-edge excitation/blue-edge emission channel (channel 1) is negligible ($T_1 \approx 0$) – meaning in the language of correction factors $\beta = 1$, $\gamma = 0$ – the uncorrected homo-FRET efficiency (T_0) can be calculated. After factorizing out the r_1 and r_2 anisotropies and taking their ratio the initial anisotropies and the rotational depolarization factors will be cancelled, leading to Eq. (24). This value has also been proven to be a minimum of homo-FRET efficiency in the non-ideal cases characterized by different rotational strengths ($\beta < 1$) and a non-vanishing residual homo-FRET ($\gamma > 0$) in the insensitive channel, i.e., $T_0 < T$. This implies that even in the lack of a detailed knowledge of the two detection channels – i.e., unknown β and γ – the simple FRET measure of T_0 given simply by an

anisotropy ratio can always be considered as a lower estimation of the real FRET efficiency.

As a computational example for the absolute homo-FRET efficiencies, the receptor trimer system of the MHCII, β_2m , and the MHCI h.c. receptors is considered in Table 1. Here T_0 and T designate the absolute homo-FRET efficiencies computed from the primarily measured r_1 and r_2 anisotropies according to Eqs. (23), (24) and δT_0 and δT their respective changes as defined in Eq. (32). The β and γ spectral correction factors taking into account that (i) lifetime rotational correlation time ratios may not be equal in the sensitive and non-sensitive channels (β), and (ii) the homo-FRET may not be perfectly vanishing in the non-sensitive channel (red-edge) (γ) have been computed in advance from the intersections and slopes of reciprocal anisotropy-surface concentration titration Perrin-plots (Eq. (32)) by the algorithm detailed in the theoretical part and in the Supporting information.

According to Table 1 Part A, all r_2 anisotropies of the singly labeled samples are systematically smaller than the corresponding r_1 anisotropies giving rise to a $\sim 10\%$ T_0 FRET efficiencies ($\bar{T}_0 = 10.9 \pm 0.8\%$), which increase upon correction ($\bar{T} = 15.1 \pm 0.6\%$). A trivial advantage of the absolute homo-FRET efficiency is the capability for measuring homo-FRET already on the singly labeled samples. Concerning sensitivity of T to the corrections, β seems to affect T more sensitively than γ . These T_0 and T values report on substantial homo-associations of the A488 dye even when single mAbs have been used for labeling the cells. A portion of the homo-association is explained by the multiple-labeling of the individual mAb molecules – i.e., labeling ratios higher than unity –, another portion by the substantial homo-associations of the MHCII and MHCI receptors expressed at high levels ($\sim 10^6$, $\sim 1.5 \times 10^6$, respectively) on the cell surface.

The resulting values in Part A have been further used with the corresponding intensities (not shown) to compute the pair-wise and triple-wise intensity averages – of β , γ , r_1 , r_2 , T_0 , and T for the computation of η , δT_0 , and δT – necessary in Parts B and C as input parameters. From Part B we learn that, while upon the simultaneous application of two different ligands r_2 systematically decreases, and r_1 stays steadily at the single labeled values. This is consistent with homo-FRET operating in the main band and vanishing at the red-edge. This same information can be obtained in an alternative quantitative form by computing the homo-FRET enhancements η_1 and η_2 , which are clear indicator of the cluster sizes. Accordingly, while η_1 computed from r_1 stays steadily close to zero ($\bar{\eta}_1 = -2.6 \pm 0.9\%$), η_2 computed from r_2 assumes values significantly different larger than zero ($\bar{\eta}_2 = 6.5 \pm 0.5\%$), albeit by not much. As to the smallness of the η_2 values, lifetime reduction upon multiple labeling may occur, which may counteract the depolarizing effect of homo-FRET (see also the part on rFLIM in the Supporting information). By ratioing the corresponding r_2 and r_1 anisotropies, T_0 (and T) have been obtained, which are substantially larger than the values ($\bar{T}_0 = 18.3 \pm 1.3\%$) belonging to the singly labeled samples ($\bar{T}_0 = 10.9 \pm 0.8\%$). Actually the T_0 (and T) values – or rather the rate constants computed as $T_0/(1 - T_0)$ – are approximately the sum of those for the corresponding singly labeled sample values. By taking also the increments in T_0 and T (δT_0 , δT) analogous to the η -s, we see that they ($\delta \bar{T}_0 = 7.0 \pm 0.8\%$) are very close to the corresponding $\eta_2 - \eta_1$ differences ($8.1 \pm 1.0\%$), informing us on the fulfillment of the law laid down in Eq. (42). The very small deviations between the corresponding δT_0 and δT values inform us about a large degree of tolerance of these quantities to the corrections with β and γ due to linearity of the formula defining T in terms of these quantities. Homo-FRET values of Part B measured on mAb-pairs report on an appearing excess homo-FRET, as compared to the single-mAbs, being each value of T_0 (and T) larger than the average T_0 (and T) for the corresponding individual mAbs ($\delta \bar{T}_0 = 7.0 \pm 0.8\%$). This behavior is explained by the fact that these receptors are substantially associated with each other. The largest T_0 (and T) obtained by labeling all the three receptors, in Part C ($\bar{T}_0 = 21.9 \pm 1.5\%$), reports on the existence of triplets of these

receptors as expected based on the pair wise associations demonstrated in Part B. Accordingly the differential increments η_2 and δT_0 are the largest in this case ($\eta_2 = 7.9 \pm 2.1\%$, $\delta T_0 = 10.6 \pm 2.9\%$).

To reveal the properties of the above quantities concerning differences in dye tethering motion and antibody arm (Fab) flexibilities we carried out analogue experiments also with Fab fragments instead of whole mAbs, and xFITC dye instead of A488. The pertinent data are shown in Tables 1s and 2s in the Supporting information. With these systems we observed essentially the same trends as for the A488-mAbs, implying that the results on the relative proximities yielded by our anisotropy ratio-based methodology are essentially label independent.

In addition to informing us about the same trends as by the case of whole mAbs, these data emphasize the utility of the homo-FRET efficiency for classifying homo-FRET on the single labeled samples made apparent by a clear dependence of the T_0 and T efficiencies on the labeling ratio of the ligands, supported by the following observation: Comparing all the T_0 and T values globally for the A488-Fab (Table 1s) and xFITC-mAb (Table 2s) cases with those for the A488-mAb case (Table 1), a clear dependence on the labeling ratio can be noticed: The FRET efficiencies are the smallest for A488-Fab case ($\bar{T}_0 = 10.4 \pm$

1.5%, $\bar{L} = 0.8 \pm 0.2$), medium for the A488-mAb case ($\bar{T}_0 = 14.6 \pm 0.8\%$, $\bar{L} = 2.5 \pm 0.4$) and the largest for the xFITC-mAb case ($\bar{T}_0 = 20.2 \pm 0.9\%$, $\bar{L} = 4.2 \pm 0.4$). Interestingly, considering the homo-FRET enhancements (η) or the differences in the homo-FRET efficiency (δT_0) the reversed order can be notified: These “differential” quantities are the smallest ($\delta \bar{T}_0 = 4.0 \pm 1.2\%$) for the largest labeling ratios (xFITC-mAb), and larger for the smaller ones ($\delta \bar{T}_0 = 7.9 \pm 1.5\%$ for A488-mAb, $\delta \bar{T}_0 = 6.8 \pm 0.5\%$ for A488-Fab). The implication of this observation is that sensitivity of homo-FRET to receptor clustering is inversely proportional to the initial size of dye clusters on the ligands themselves dictated by their labeling ratio.

4.6. rFLIM on receptor trimers

As an independent control for equipment, the above experiments on the receptor trimers have been done also on a polarized fluorescence lifetime imaging microscope working in the frequency domain (rFLIM). In addition to the phase and modulation lifetime information relative anisotropy ($\eta = \delta r/r$), modulation amplitude ($\delta Y_{ac}/Y_{ac}$), and “differential tangent” ($\delta \tan(\Delta\Phi)/\tan(\Delta\Phi)$) of the multiply labeled samples as

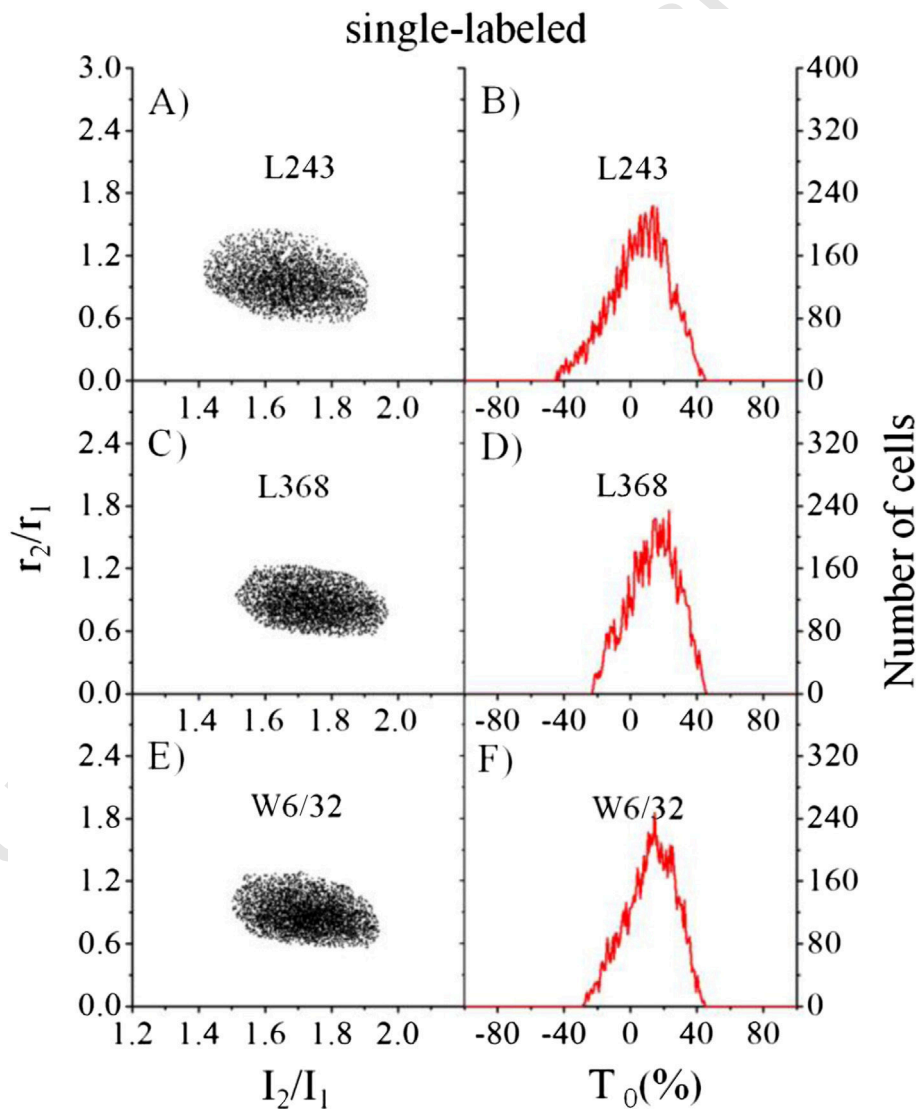


Fig. 8. Representative flow cytometric dot-plots and histograms measured on the receptor trimer MHCII- β_2 m-MHCI h.c. singly labeled with the indicated A488-Fabs. Panels A, C, E: Anisotropy ratio (r_2/r_1) vs. intensity ratio (I_2/I_1) scatter-plots. The gradual decrease of r_2/r_1 with increasing I_2/I_1 is an indication of increasing homo-FRET. Panels A, C, E: Absolute homo-FRET efficiency T_0 distributions computed with the r_1 and r_2 distributions. Pertinent statistical data are found in Table 1s, Part A, Supporting information.

868 compared to the pertinent single labeled intensity averages have been
 869 computed. In addition to proving the presence of homo-FRET between
 870 the labels and justifying the trends found with flow cytometry, the
 871 data also shed light a reduction of lifetime ($\sim 5\text{--}10\%$) upon increasing
 872 the number of labels. This lifetime reduction – supposedly due to an
 873 increased rate of FRET towards dim dye complexes – **mitigates** the
 874 depolarization of homo-FRET and **tends** to reduce the magnitudes of
 875 relative anisotropy changes (η). Please see the details and data in
 876 Tables 3s, and 4s in the Supporting information.

877 4.7. Flow cytometric dot-plots and histograms measured on the receptor 878 trimer multiply labeled with A488-Fabs

879 Representative anisotropy ratio (r_2/r_1) vs. intensity ratio (I_2/I_1),
 880 intensity (I_1, I_2) dot-plots, and computed T_0 histograms are shown in
 881 Figs. 8–10 for the single-, double- and triple-labeled cases, respectively,
 882 of the MHCII- β_2m -MHCII h.c. receptor trimer. The r_2/r_1 vs. I_2/I_1 dot-plots
 883 demonstrate the directed migration FRET amongst the heterogeneous
 884 sites. The gradual decrease of the anisotropy ratio with increasing intensity
 885 ratio is due to that fact that FRET happens towards the lower energy
 886 sites. According to Figs. 8–10 Panels A, C, and E, and Fig. 10 Panel A, the

r_2/r_1 vs. I_2/I_1 dot-plots sensitively change as the number of applied
 887 labels increases. While I_2/I_1 increases, r_2/r_1 decreases with increasing
 888 number of applied labels, the smallest effect being observed on the
 889 singly labeled samples (Fig. 8 Panels A, C, E) and the largest one on
 890 the triply labeled one (Fig. 10 Panel A). An interesting feature is that
 891 the slope of the fitting trend line shows a systematic decrease as the
 892 number of labels is increased, an offset property supposedly due to
 893 the fact that the receptors are already homo-associated when they are
 894 singly-labeled with the Fabs. In Figs. 8–10 also shown are the corre-
 895 sponding homo-FRET efficiency histograms (T_0). At the first site it is
 896 clearly visible that the width of the T_0 distribution strongly depends
 897 on the signal-to-noise ratio: being largest on the single-labeled samples
 898 (Fig. 8) and the smallest on the triple-labeled one (Fig. 10). Additional
 899 useful representations are the r_1 vs. I_2/I_1 and the r_2 vs. I_2/I_1 dot-plots
 900 (Fig. 10, Panels C, D). Remarkable feature is that while r_2 decreases
 901 steadily with increasing I_2/I_1 , r_1 shows a little increase. A possible reason
 902 can be that with red shifting the emission spectrum (increase in I_2/I_1)
 903 the absorption is also shifted towards longer wavelengths implying a
 904 reduction in homo-FRET and a concomitant increase in anisotropy r_1 ,
 905 i.e., a further manifestation of the red-edge effect. If now the anisotropy
 906 ratio r_2/r_1 is plotted against the I_1 and I_2 intensities (Fig. 10, Panels E, F),
 907

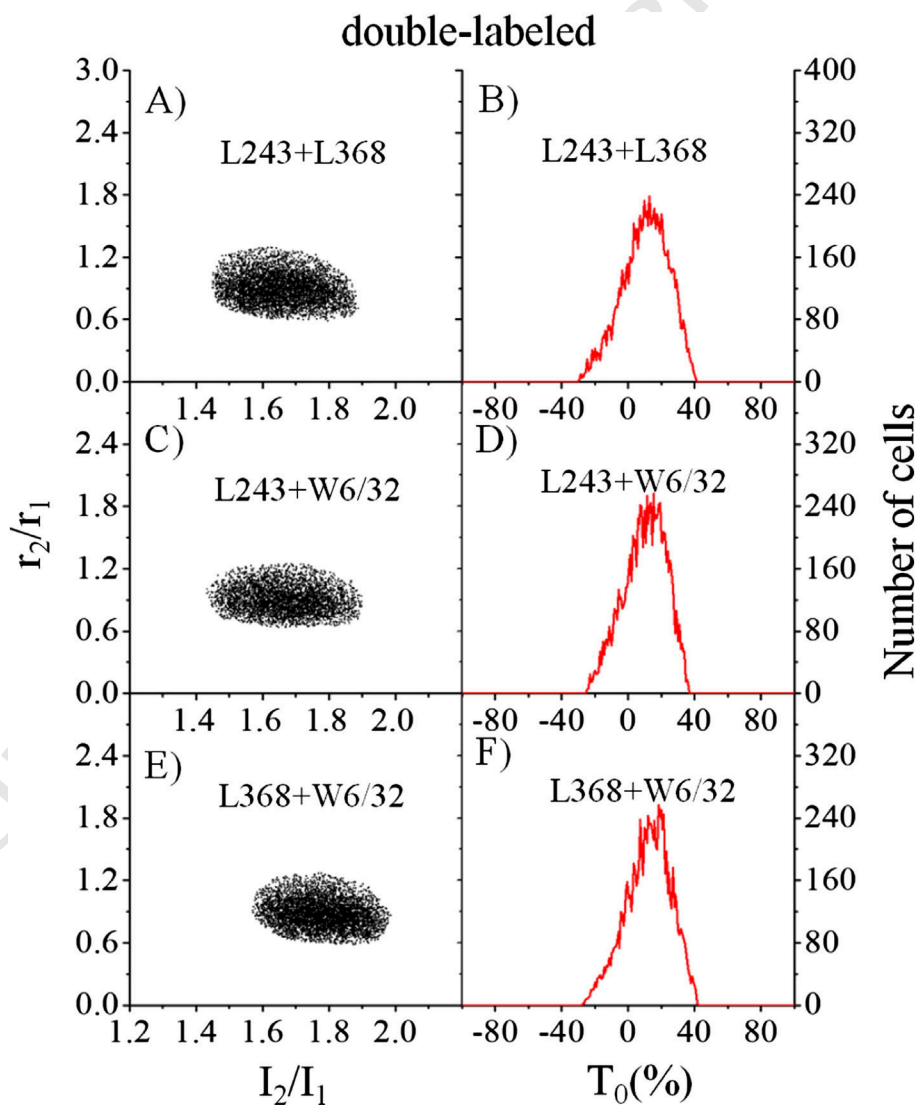


Fig. 9. Representative flow cytometric dot-plots and histograms measured on the receptor trimer MHCII- β_2m -MHCII h.c. doubly labeled with the indicated A488-Fabs. Panels A, C, E: Anisotropy ratio (r_2/r_1) vs. intensity ratio (I_2/I_1) scatter-plots. The gradual decrease of r_2/r_1 with increasing I_2/I_1 is an indication of increasing homo-FRET. Panels A, C, E: Absolute homo-FRET efficiency T_0 distributions computed with the r_1 and r_2 distributions. Pertinent statistical data are found in Table 1s, Part B, Supporting information.

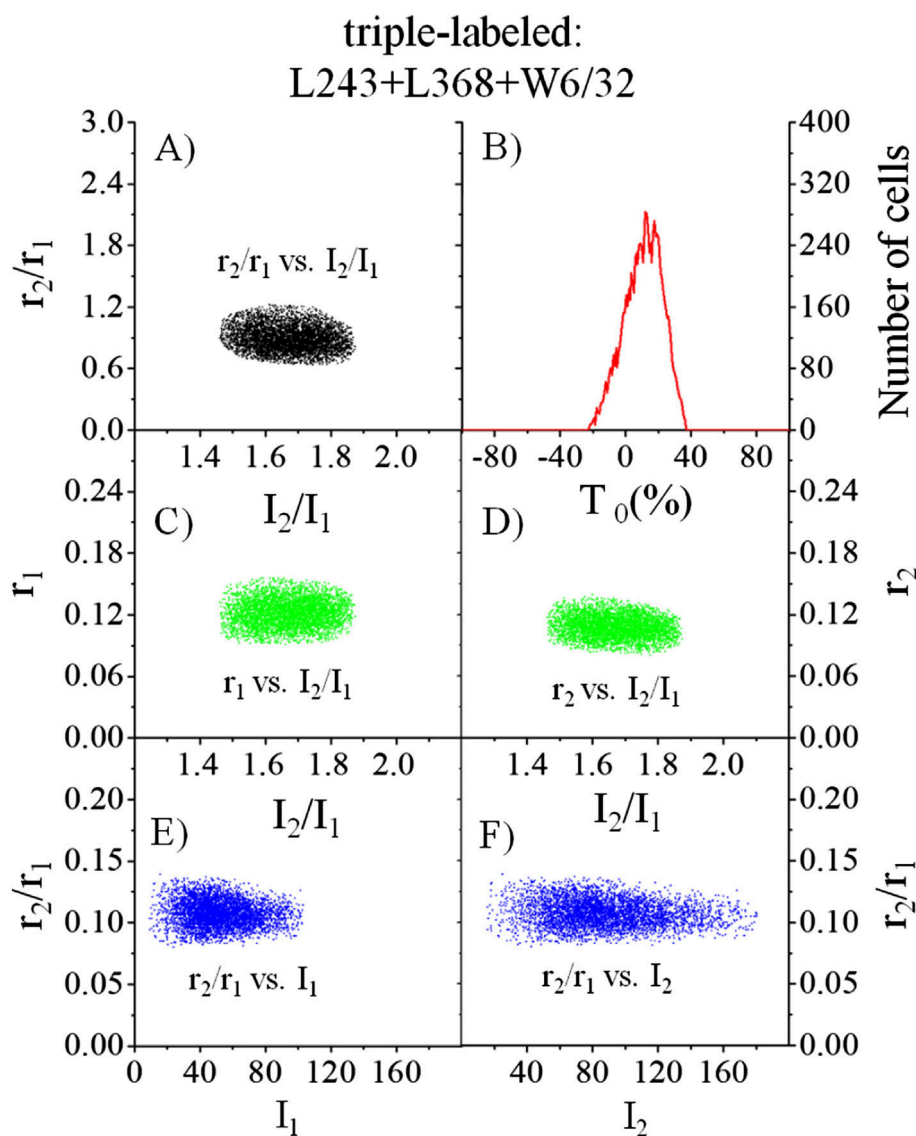


Fig. 10. Representative flow cytometric dot-plots and histograms measured on the receptor trimer MHCII- β_2m -MHCI h.c. triply labeled with the indicated A488-Fabs. Panel A: Anisotropy ratio (r_2/r_1) vs. intensity ratio (I_2/I_1) scatter-plot. The gradual decrease of r_2/r_1 with increasing I_2/I_1 is an indication of increasing homo-FRET. Panel B: Absolute homo-FRET efficiency T_0 distribution computed with the r_1 and r_2 distributions. Panel C: Green channel anisotropy (r_1) vs. intensity ratio (I_2/I_1) scatter-plot. Panel D: Red channel anisotropy (r_2) vs. intensity ratio (I_2/I_1) scatter-plot. Panel E: Anisotropy ratio (r_2/r_1) vs. green channel intensity (I_1) scatter-plot. Panel F: Anisotropy ratio (r_2/r_1) vs. red channel intensity (I_2) scatter-plot. Pertinent statistical data are found in Table 1s, Part A, Supporting information.

then while a reduction in r_2/r_1 can be seen with increasing I_2 , practically no change can be seen with increasing I_1 .

5. Discussion

5.1. Red-edge effects with tethered fluorophores

Although originally it has been described for fairly viscous and rigid media, we observed the operation of inhomogeneous broadening and the associated red-edge effects for highly mobile tethered dyes. The existence of this phenomenon in this situation suggests a long-lasting stability of the solvent microenvironments around the fluorophores, i.e., environmental relaxation times falling on the scale of fluorescence lifetime or longer. This observation is in good accordance with the previously reported ~ 0.4 rotational strength (τ/ϕ_{rot}) of the tethered dyes – implying a 10-nsec rotational correlation time (ϕ_{rot}) for a 4-nsec lifetime (τ) – observed with FRET-resolved donor anisotropy measurements [35], which has also been conformed with rFLIM ($\tau^{ph}/\phi_{rot} =$

0.42 ± 0.04 , as computed from data on single labeled cells in Tables 3s, and 4s in the Supporting information). The existence of inhomogeneous broadening also implies that homo-FRET does not exist in the strict sense of the word even for chemically identical dyes, because the unavoidable environmental heterogeneity endows them with spectral heterogeneity unless the environmental relaxation time is much smaller than the fluorescence lifetime. Site-selective spectroscopy offered the opportunity for the optimization of the excitation and detection conditions for establishing a homo-FRET sensitive and an insensitive detection channel [18]. The two main characteristic spectral manifestations of inhomogeneous broadening exploited in the optimization are that homo-FRET is favored for main-band excitation and red-edge emission, and suppressed for red-edge excitation and blue-edge emission. After establishing the FRET-sensitive and insensitive channels accordingly – 488 nm excitation/640 nm emission, and 514 nm excitation/535 nm emission – we were able to separate the rotational and FRET-contributions to the depolarization of fluorescence anisotropy by dropping out the rotational component via ratioing the anisotropies of the two detection channels. However, the homo-FRET efficiency T_0 defined this way (Eq. (24)) can

be considered only as an approximation, because it rests on the assumption of identical τ/ϕ_{rot} ratios (“rotation strengths”) in the two channels and zero residual FRET in the insensitive channel. For correcting these shortcomings the spectral correction factors β and γ have been introduced (Eqs. (17), (18)) in the definition of another, the “true” homo-FRET efficiency T (Eq. (23)), based on linear fitting of the reciprocal anisotropy vs. surface concentration Perrin-plots (Eq. (30)). Nevertheless, the usefulness of the T_0 is stressed by the fact that it can always be considered as a lower approximation of the true homo-FRET efficiency – i.e., $T_0 \leq T$ – also in those cases when β and γ are not known and T cannot be computed.

The elaboration of this method was substantially inspired by the publication of A. Squire et al. [10]. They called the attention for the possibility for separating the rotational and FRET contributions to the depolarization of anisotropy by utilizing red-edge absorption and illustrated the method with visible engineered proteins (VFP-s). Our intention was to generalize their approach by (i) choosing a much wider class of labels – such as surface tethered dyes – possessing also a substantially larger degree of tethering motion compared to VFP, which is practically immobile, (ii) taking into account not only the absorption red-edge, but also the emission blue-edge effect for optimization of homo-FRET suppression and detection, (iii) giving a theoretically firm basis for the separation of effects of homo-FRET and rotation by factorizing anisotropy according to Soleillet's theorem [22–24], (iv) constructing an optical scheme which enables a “simultaneous” – up to the 30- μs delay-time of the green and blue laser lines in the flow cytometer, Fig. 2 – detection of the two anisotropies, which is necessary for a real-time monitoring of receptor dynamics.

5.2. Calibration of absolute homo-FRET determination

An important feature of our absolute homo-FRET efficiency determination is that it does not require a calibration of the different sensitivities of the green and red channels, i.e., the problem of finding the best “ α -factor” for FRET is avoided [36] here. This problem is eliminated by the fact that two anisotropies are compared, which are absolute quantities being computed with intensity ratios. However, for the accurate FRET-efficiency calculation – according to Eq. (24) for T_0 – the knowledge of the lifetime-rotational correlation time ratio in the two detection channels or at least their approximate equality is required, besides the condition that homo-FRET should be zero in the insensitive channel. For a refinement of our methodology, we checked these properties for our mAbs, and determined the β and γ quantities (see Fig. 5s in the Supporting information) describing the relative rotational strengths and homo-FRET rates in the two detection channels. We found β to be close to unity ($\beta > 94\%$), and γ to be close zero ($\gamma < 13\%$), independently of the type of the dye-carrier ligand and its labeling ratio, indicating that the A488-mAb systems are close to the ideal at the 488 and 514.5 nm excitation wavelengths.

According to direct lifetime measurements of the same mAbs with FLIM, the near equal rotational strengths manifested in β close to unity is corroborated by also the observation that the lifetimes measured in the red and green channels are approximately equal with each other (see Fig. 6s in the Supporting information).

5.3. Homo-FRET efficiency and enhancement

Absolute homo-FRET efficiency T_0 (and T) is distinct from the homo-FRET enhancement factors (η_2) introduced earlier with the receptor trimers (Fig. 3). Although, the pair-wise and triple-wise homo-FRET-enhancements η_2 shown in Fig. 3 give the same results qualitatively, they are only relative values and they cannot be used for describing homo-FRET on the single-labeled samples. While the homo-FRET enhancement factors (η_2) represent the change of homo-FRET efficiency caused by the application of a 2nd label (mAb, Fab), T_0 represents the total homo-FRET efficiency, i.e., the amount of homo-FRET before a

2nd label (“starting homo-FRET”), plus the homo-FRET increment caused by binding of a 2nd label. Alternatively, η_2 means the differential change in absolute homo-FRET efficiency caused by the introduction of a 2nd label: $\eta_2 \approx T_0$ (after 2nd label) – T_0 (before 2nd label), see also Eqs. (32), and (42).

5.4. Intensity ratio-based homo-FRET efficiencies

In addition to the anisotropy-based absolute homo-FRET efficiencies (T_0 , T), the observation that homo-FRET leads to a gradual shift of emission wavelength to the red (Figs. 5, 6) may offer another possibilities for characterizing homo-FRET: An intensity-based quantity E_1 may also be introduced. E_1 may be defined as the relative change between the I_2 and I_1 intensities when the main-band (2nd channel) and the red-edge (1st channel) excitations are compared:

$$E_1 \equiv \alpha \cdot I_2/I_1 - 1, \quad (43)$$

where α is a correction factor taking into account the different sensitivities of the detection channels [36]. As a kind of calibration, α can be fixed by making equal the two FRET efficiencies defined according to Eqs. (24), and (43). This approach is supported by the observation that the r_2/r_1 ratio is approximately a linearly decreasing function of I_2/I_1 (Figs. 8–10) leading to approximately the same α values independently of the receptor for a given optical adjustment of the cytometer. By computing the means of histograms of the α quantity defined as

$$\alpha \equiv (2 - r_2/r_1)/(I_2/I_1), \quad (44)$$

we obtained: 0.65 ± 0.006 , for the 7 samples displayed in Figs. 8–10. Besides α histogram linear fitting of the r_2/r_1 vs. I_2/I_1 correlation diagrams could be used.

Alternatively, another quantity E_2 can also be defined as a relative change of the $I_{\text{red}}/I_{\text{green}}$ intensity ratio (like the I_2/I_1 ratio on Figs. 5, 6, and 1s, 2s in the Supporting information) when the main-band (2nd channel) and the red-edge (1st channel) excitations are compared (“differential intensity red shift”):

$$E_2 \equiv \left(I_{\text{red}}/I_{\text{green}} \right)_1 / \left(I_{\text{red}}/I_{\text{green}} \right) - 1. \quad (45)$$

This quantity does not need calibration, the cost of which is the need for 2 extra detection channels: green detection at the main band ($I_{\text{green},2}$), and red detection at the red-edge ($I_{\text{red},1}$).

5.5. Applicability of the method

This methodology enables the possibility for a quick – minute level – assessment of an otherwise only hardly accessible parameter, the absolute homo-FRET efficiency as freed from rotation effects in flow condition. Doing this in a single measuring act, the method is capable for real-time monitoring of receptor dynamics manifested in changing proximities and rotational mobility by using only a single type of dye. This same information can also be assessed by controlling fluorophore concentration via changing the amount of dye-tagged ligands for labeling of receptors, photobleaching and photon-saturation of the dye [4–9, 12–14]. However, these latter possibilities demand multiple samples, longer exposition times, or high illumination intensities precluding the real-time observations in living conditions in a flow cytometer. They are most suitable for microscopic applications. With this approach, we focused to flow cytometry, because this is the platform for a multiparametric quick assessment of cell-by-cell level correlations between parameters as diverse as inter-receptor proximities, receptor mobilities, ion concentrations, and membrane potential [40,41]. Amongst the outstanding properties of flow cytometry is its high statistical precision, making possible investigations on weakly expressed receptors on very small cell populations, consequently the early diagnosis of diseases.

Apart from flow cytometry, the method can also be applied in fluorescence microscopes capable for dual-anisotropy detection, e.g., via a quadrant image splitter making possible separation of light according to color and polarization. Furthermore, other types of receptors, not necessarily expressed on the cell surface and dye-targeting ligands other than mAbs could also be applied.

As to the utility of fluorophores, the major requirement is the high enough r_0 limiting anisotropy – in addition the natural requirement for the small Stokes-shift for the large spectral overlap – to ensure adequate dynamic range for reduction of anisotropy due to homo-FRET. Further requirements are a substantial rotation on the time-scale of fluorescence and a tendency for inhomogeneous broadening. For non-rotating, stiff chromophores – such as engineered visible proteins – this method is meaningless, albeit these systems are amongst the best candidates with respect to the detectability of homo-FRET. A large class of fluorophores conjugatable to carriers, with chromophore groups directly exposed to the environment, amongst which the polarity dyes having large environmental sensitivity, seems to be amongst the best candidates because these have both rotational freedom and inhomogeneous broadening. Quantum dots may also be applicable, although their environmental sensitivity could be smaller due to shielding by a capping layer. As to studies of mosaicism of the lipid bilayer, morphology of membrane domains may be monitored by measurement of homo-FRET between e.g., the DPH, or BODIPY dyes [42], which may possess substantial rotational mobility besides homo-FRET.

Another advantage of the ratio-based homo-FRET determination may be that it is free from lifetime artifacts. Detecting that homo-FRET could be hindered by a concentration and intensity dependent lifetime reduction as observed by us – see the lifetime values in Tables 3s, and 4s as function of labeling ratio and the number of ligands added together and in [36] – and by others for dyes [42–45], and recently by Nedbal et al. for VFP [46]. Supposedly weakly fluorescing dye associates, “dim complexes” are behind this observation, which may reduce lifetime by self-quenching. This may increase fluorescence anisotropy, and mitigate the depolarizing effect of homo-FRET. This may explain that we observed rather modest homo-FRET enhancements (~10–15%) for the pairs of the receptor trimer [4] for which much larger hetero-FRET efficiencies (~20–30%) were observed earlier. In the present formalism based on anisotropy ratio, however, this effect drops out, because both the numerator and de-numerator are inflated by the same way.

As to the technical realization of the method, the main requirement is to ensure simultaneously the negligible homo-FRET and the high enough fluorescence signal at the red edge. By inspecting the homo-FRET rate curves for the 2nd fluorescence channel (A_2) – the red curves of Fig. 5s Panels A–C–E in the Supporting information – we can see that the homo-FRET rate at the red-edge (514.5 nm) is practically zero. This implies that the homo-FRET insensitive signal can also be measured in the same, red fluorescence channel in which the sensitive one is measured, depending on the signal level dictated by biological and technical factors such as receptor expression level and light intensity for excitation.

6. Conclusion

Red-edge effects have been demonstrated for the highly mobile mAb-tethered dyes targeted to membrane receptors. By exploiting site-selective spectroscopy, FRET-sensitive and insensitive channels have been established, which made possible an absolute determination of homo-FRET efficiency by ratioing the fluorescence anisotropies measured in the two channels. Although accurate determination of absolute homo-FRET efficiency requires – besides the high-enough limiting anisotropy r_0 – a careful control of spectral characteristics such as relative homo-FRET rates (γ -factor) and relative rotation strengths (β -factor) on the actual FRET-sample, the homo-FRET efficiency T_0 computed with a simple ratio of the anisotropies in the homo-FRET-sensitive and

insensitive channels serves as a minimum for the true homo-FRET efficiency even in the lack of this spectral information. Based on the fact that the two anisotropies simultaneously detected, the method may be exploited in real-time monitoring of dynamical processes like conformational changes where both rotational mobility and inter-dye proximity can equally be affected. Although the method has been demonstrated in the context of flow cytometry it can be realized also in microscopes equipped with dual-laser excitation and dual-channel anisotropy detection facilities.

7. Uncited references

[33,37,38,39]

Transparency Document

The Transparency document associated with this article can be found, in the online version.

Acknowledgements

Financial support for this work was provided by TÁMOP-4.2.2.A-11/1/KONV-2012-0045 project co-financed by the European Union and the European Social Fund, and OTKA Bridging Fund support OSTRAT/810/213 by the University of Debrecen. The authors are indebted to Dr. T. M. Jovin for using FLIM in the framework of a short term EMBO fellowship, ASTF No 201–06, to the Max Planck Institute for Biophysical Chemistry, Department of Molecular Biology, Göttingen to L. B. Thanks are due to Dr. M. Bagdány, for helpful discussions on FRET and his overview of possible applications of FRET in molecular genetics.

Appendix A. Supplementary data

Supplementary data to this article can be found online at <http://dx.doi.org/10.1016/j.bbamcr.2015.02.001>.

References

- [1] E.A. Jares-Erijman, T.M. Jovin, FRET imaging, *Nat. Biotechnol.* 21 (11) (2003) 1387–1395.
- [2] F.T.S. Chan, C.F. Kaminski, G.S. Kaminski Schierle, HomoFRET fluorescence anisotropy imaging as a tool to study molecular self-assembly in live cells, *ChemPhysChem* (2010). <http://dx.doi.org/10.1002/cphc.201000833>.
- [3] L.W. Runnels, S.F. Scarlata, Theory and application of fluorescence homotransfer to mellitin oligomerization, *Biophys. J.* 69 (1995) 1569–1583.
- [4] L. Bene, J. Szöllösi, G. Szentesi, L. Damjanovich, R. Jr, T.A. Gáspár, S. Damjanovich Waldmann, Detection of receptor trimers on the cell surface by flow cytometric fluorescence energy homotransfer measurements, *Biochim. Biophys. Acta Mol. Cell Res.* 1744 (2005) 176–198.
- [5] E.K.L. Yeow, A.H.A. Clayton, Enumeration of oligomerization states of membrane proteins in living cells by homo-FRET spectroscopy and microscopy: theory and application, *Biophys. J.* 92 (2007) 3098–3104.
- [6] Á. Szabó, G. Horváth, J. Szöllösi, P. Nagy, Quantitative characterization of the large-scale association of ErbB1 and ErbB2 by flow cytometric homo-FRET measurements, *Biophys. J.* 95 (2008) 2086–2096.
- [7] A.N. Bader, E.G. Hofman, J. Voortman, P.M.P. Van Bergen en Henegouwen, H.C. Gerritsen, Homo-FRET imaging enables quantification of protein cluster sizes with subcellular resolution, *Biophys. J.* 97 (2009) 2613–2622.
- [8] S. Ganguly, A.H.A. Clayton, A. Chattopadhyay, Organization of higher-order oligomers of the serotonin 1A receptor explored utilizing homo-FRET in live cells, *Biophys. J.* 100 (2011) 361–368.
- [9] A.M. Melo, A. Fedorov, M. Prieto, A. Coutinho, Exploring homo-FRET to quantify the oligomer stoichiometry of membrane-bound proteins involved in a cooperative partition equilibrium, *Phys. Chem. Chem. Phys.* (2014). <http://dx.doi.org/10.1039/C4CP00060A>.
- [10] A. Squire, P.J. Verveer, O. Rocks, P.I.H. Bastiens, Red-edge anisotropy microscopy enables dynamic imaging of homo-FRET between green fluorescent proteins in cells, *J. Struct. Biol.* 147 (2004) 62–69.
- [11] P.I.H. Bastiens, A. van Hoek, J.A.E. Benen, J.-C. Brochon, A.J.W.G. Visser, Conformational dynamics and intersubunit energy transfer in wild-type and mutant lipamide dehydrogenase from *Azotobacter vinelandii*, *Biophys. J.* 63 (1992) 839–853.
- [12] A.H.A. Clayton, Q.S. Hanley, D.J. Arndt-Jovin, V. Subramaniam, T.M. Jovin, Dynamic fluorescence anisotropy imaging microscopy in the frequency domain (rFLIM), *Biophys. J.* 83 (2002) 1631–1649.

- 1186 [13] D.S. Lidke, P. Nagy, B.G. Barisas, R. Heintzmann, J.N. Post, K.A. Lidke, A.H. Clayton, D.J.
1187 Arndt-Jovin, T.M. Jovin, Imaging molecular interactions in cells by dynamic and
1188 static fluorescence anisotropy (rFLIM and emFRET), *Biochem. Soc. Trans.* 31 (2003)
1189 1020–1027.
- 1190 [14] M. Beutler, K. Makrogianneli, R.J. Vermeij, M. Keppler, T. Ng, T.M. Jovin, R.
1191 Heintzmann, satFRET: estimation of Förster resonance energy transfer by acceptor
1192 saturation, *Eur. Biophys. J.* 38 (1) (2008) 69–82.
- 1193 [15] J.R. Lakowicz, Dynamics of solvent and spectral relaxationCh. 7 Principles of Fluorescence
1194 Spectroscopy, 3rd ed.Springer, 2006, pp. 237–275.
- 1195 [16] B. Valeur, Resonance energy transfer and its applicationsChapter 9 Molecular
1196 Fluorescence. Principles and Applications, Wiley-VCH, Weinheim, 2002, pp. 247–272.
- 1197 [17] S. Mukherjee, A. Chattopadhyay, Wavelength-selective fluorescence as a novel tool to
1198 study organization and dynamics in complex biological systems, *J. Fluoresc.* 5 (3)
1199 (1995) 237–246.
- 1200 [18] A.P. Demchenko, Site-selective red-edge effectsCh. 4 in *Methods Enzymol.* 450
1201 (2008) 59–78.
- 1202 [19] A.P. Demchenko, The red-edge effects: 30 years of exploration, *Luminescence* 17
1203 (2002) 19–42.
- 1204 [20] N.A. Nemkovich, A.N. Rubinov, V.I. Tomin, Inhomogeneous broadening of electronic
1205 spectra of dye molecules in solutionsChapter 8 in: J.R. Lakowicz (Ed.), *Topics in*
1206 *Fluorescence Spectroscopy, Principles, Vol. 2*, Plenum Press, New York, London,
1207 1991, pp. 367–428.
- 1208 [21] R. Gáspár Jr., P. Bagossi, L. Bene, J. Matkó, J. Szöllösi, J. Tözsér, L. Fésüs, T.A.
1209 Waldmann, S. Damjanovich, Clustering of class I HLA oligomers with CD8 and
1210 TCR: three-dimensional models based on fluorescence resonance energy transfer
1211 and crystallographic data, *J. Immunol.* 166 (2001) 5078–5086.
- 1212 [22] R.E. Dale, J. Eisinger, W.E. Blumberg, The orientational freedom of molecular probes.
1213 The orientation factor in intramolecular energy transfer, *Biophys. J.* 26 (1979)
1214 161–194.
- 1215 [23] B.W. van der Meer, Orientational aspects in pair energy transfer, in: D.L. Andrews,
1216 A.A. Demidov (Eds.), *Resonance Energy Transfer*, J. Wiley & Sons, New York, 1999,
1217 pp. 151–172.
- 1218 [24] B.W. van der Meer, Kappa-squared: from nuisance to new sense, *Rev. Mol.*
1219 *Biotechnol.* 82 (2002) 181–196.
- 1220 [25] T. Hori, T. Uchiyama, M. Tsudo, H. Umadome, H. Ohno, S. Fukuhara, K. Kita, H.
1221 Uchino, Establishment of an interleukin 2-dependent human T cell line from a
1222 patient with T cell chronic lymphocytic leukemia who is not infected with human
1223 T cell leukemia/lymphoma virus, *Blood* 70 (1987) 1069–1073.
- 1224 [26] C.J. Barnstable, W.F. Bodmer, G. Brown, G. Galfré, C. Milstein, A.F. Williams, A. Ziegler,
1225 Production of monoclonal antibodies to group A erythrocytes, HLA and other human
1226 cell surface antigens—new tools for genetic analysis, *Cell* 14 (1978) 9–20.
- 1227 [27] M. Tanabe, M. Sekimata, S. Ferrone, M. Takiguchi, Structural and functional analysis
1228 of monomorphic determinants recognized by monoclonal antibodies reacting with
1229 HLA class I alpha 3 domain, *J. Immunol.* 148 (1992) 3202–3209.
- 1230 [28] M. Edidin, T. Wei, Lateral diffusion of H-2 antigens on mouse fibroblasts, *J. Cell Biol.*
1231 95 (1982) 458–462.
- 1232 [29] E.G. Spack Jr., B. Packard, M.L. Wier, M. Edidin, Hydrophobic adsorption chromatography
1233 to reduce nonspecific staining by rhodamine-labeled antibodies, *Anal.*
1234 *Biochem.* 158 (1986) 233–237.
- [30] S. De Petris, Immunoelectron microscopy and immunofluorescence in membrane
1235 biology, in: E.D. Korn (Ed.), *Methods in Membrane Biology*, vol 9, Plenum Press,
1236 New York, 1978, pp. 1–201.
- [31] J.R. Lakowicz, Fluorescence anisotropyCh. 10. Principles of Fluorescence Spectroscopy,
1237 3th ed.Springer, 2006, pp. 353–381.
- [32] T.M. Jovin, Fluorescence polarization and energy transfer: theory and application, in:
1238 M. Melamed, P. Mullaney, M. Mendelsohn (Eds.), *Flow Cytometry and Sorting*,
1239 J. Wiley & Sons, New York, 1979, pp. 137–165.
- [33] G. Szentesi, G. Horváth, I. Bori, G. Vámosi, J. Szöllösi, R. Gáspár, S. Damjanovich, A.
1240 Jenei, L. Mátyus, Computer program for determining fluorescence energy transfer
1241 efficiency from flow cytometric data on a cell-by-cell basis, *Comput. Methods*
1242 *Prog. Biomed.* 75 (2004) 201–211.
- [34] R.A. Badley, Fluorescent probing of dynamic and molecular organization of biological
1243 membranesCh. 3 in: E.L. Wehry (Ed.), *Modern Fluorescence Spectroscopy*, vol. 2,
1244 Heyden, 1976, pp. 91–168.
- [35] L. Bene, M.J. Fulwyler, S. Damjanovich, Detection of receptor clustering by flow cyto-
1245 metric fluorescence anisotropy measurements, *Cytometry* 40 (2000) 292–306.
- [36] L. Bene, T. Ungvári, R. Fedor, Sasi-Szabó László, L. Damjanovich, Intensity
1246 correlation-based calibration of FRET, *Biophys. J.* 105 (2013) 1–13.
- [37] Q.S. Hanley, V. Subramaniam, D.J. Arndt-Jovin, T.M. Jovin, Fluorescence lifetime
1247 imaging: multi-point calibration, minimum resolvable differences, and artifact
1248 suppression, *Cytometry* 43 (2001) 248–260.
- [38] A. Esposito, H.C. Gerritsen, F.S. Wouters, Fluorescence lifetime heterogeneity resolu-
1249 tion in the frequency domain by lifetime moments analysis, *Biophys. J.* 89 (2005)
1250 4286–4299.
- [39] C. Luengo, B. Rieger, M. van Ginkel, G.M.P. van Kempen, L.J. van Vliet, DIPimage: A
1251 Scientific Image Processing Toolbox for MATLAB. Delft Univ. Technol., Delft, The
1252 Netherlands, <http://www.qi.tnw.tudelft.nl/DIPlib1999> (Online available).
- [40] E. Gross, R.S. Bedlack, L.M. Loew, Dual-wavelength ratiometric fluorescence mea-
1253 surement of the membrane dipole potential, *Biophys. J.* 67 (1994) 208–216.
- [41] A.S. Klymchenko, G. Duportail, Y. Mély, A.P. Demchenko, Ultrasensitive two-color
1254 fluorescence probes for dipole potential in phospholipid membranes, *Proc. Natl.*
1255 *Acad. Sci. U. S. A.* 100/20 (2003) 11219–11224.
- [42] M. Kerker, M.A. Van Dilla, A. Brunsting, J.P. Kratochvil, P. Hsu, D.S. Wang, J.W.
1256 Gray, R.G. Langlois, Is the central dogma of flow cytometry true: that fluores-
1257 cence intensity is proportional to cellular dye content? *Cytometry* 3/2 (1982)
1258 71–78.
- [43] T. Hirschfeld, Quantum efficiency independence of the time integrated emission
1259 from a fluorescent molecule, *Appl. Opt.* 15/12 (1976) 3135–3139.
- [44] C. Deka, B.E. Lehnert, N.M. Lehnert, G.M. Jones, L.A. Sklar, J.A. Steinkamp, Analysis of
1260 fluorescence lifetime and quenching of FITC-conjugated antibodies on cells by
1261 phase-sensitive flow cytometry, *Cytometry* 25 (1996) 271–279.
- [45] R.I. MacDonald, Characteristics of self-quenching of the fluorescence of lipid-
1262 conjugated rhodamine in membranes, *J. Biol. Chem.* 265/23 (1990) 13533–13539.
- [46] J. Nedbal, V. Visitkul, E. Ortiz-Zapater, G. Weitsman, P. Chana, D.R. Matthews, T. Ng,
1263 S.M. Ameer-Beg, Time-domain microfluidic fluorescence lifetime flow cytometry for
1264 high-throughput Förster resonance energy transfer screening, *Cytometry A* (2014).
1265 <http://dx.doi.org/10.1002/cyto.a.22616>.